Elsevier Editorial System(tm) for Geomorphology
Manuscript Draft

Manuscript Number:

Title: Geomorphic and stratigraphic evidence of Quaternary diapiric activity enhanced by fluvial incision. Navarrés salt wall and graben system, SE Spain

Article Type: Research Paper

Keywords: Salt tectonics, erosional unloading, diapiric geomorphology, deformation rates, gravitational faulting

Corresponding Author: Dr. Francisco Gutierrez, Geology

Corresponding Author's Institution: Universidad de Zaragoza

First Author: Francisco Gutierrez, Geology

Order of Authors: Francisco Gutierrez, Geology; Jorge Sevil; Pablo G. Silva; Eduard Roca; Frederic Escosa

Abstract: The structural and stratigraphic features associated with salt structures have received extensive attention. However, there is limited work on the geomorphic and Quaternary record of diapiric activity despite its practical implications (e.g., salt and hydrocarbon extraction, geostorage activities). This work analyses the Quaternary geomorphic and stratigraphic evidence of diapiric activity in the Navarrés salt wall (SE Spain), developed along the axis of a Neogene graben. This salt system is located in a region characterized by a peculiar network of orthogonal grabens that control the drainage network. The protruding salt walls are spatially associated with the erosionally unloaded and deeply entrenched graben sections situated close to the regional base level. Evidence of recent/current activity in the Navarrés salt wall include: (1) internally drained areas in a marginal withdrawal basin with long-sustained Quaternary deposition; (2) distorted drainage network (defeated and deflected streams, wind gaps, knickpoints, changes in fluvial style), which changed from an initial axial longitudinal pattern to a longitudinal marginal distribution at the flanks of the salt wall; (3) development of diapiric fault scarps at the edge of the salt wall; (4) tilted terraces dipping away from the salt wall and locally thickened. The available data indicate along-strike variability in the deformation style and long-term vertical deformation rates. These range from ≤0.09 mm/yr, to significantly higher values (>0.2-0.4 mm/yr) in the section where the salt wall displays a more prominent relief and is affected by deep fluvial entrenchment. The regional analysis and the characterization of the Navarrés salt wall suggest that active diapirism in the region is enhanced by erosional unloading related to fluvial entrenchment, which expands from the regional base level through the upstream propagation of an incision wave.

Suggested Reviewers: Amos Frumkin
msamos@mscc.huji.ac.il
Extensive experience on active diapirs, Israel

Mehdi Zarei
zareim@shirazu.ac.ir
Mehdi Zarei, zareim@shirazu.ac.ir, extensive experience on active diapirs, Zagros Mountains

Jiri Bruthans
bruthans@natur.cuni.cz
Jiri Bruthans, bruthans@natur.cuni.cz, extensive experience on active diapirs, Zagros Mountains

Research Data Related to this Submission

There are no linked research data sets for this submission. The following reason is given:
Data will be made available on request

Dear Editor,

Please, find uploaded in the electronic system the followingcontribution for its submission to Geomorphology:

Geomorphic and stratigraphic evidence of Quaternary diapiric activity enhanced by fluvial incision. Navarrés salt wall and graben system, SE Spain

Authored by: Francisco Gutiérrez, Jorge Sevil, Pablo Silva, Eduard Roca, Frederic Escosa

The paper documents and assesses evidence of Quaternary diapiric activity in a salt wall of eastern Spain, and discusses the role played by erosional unloading related to fluvial incision on salt flowage.

Yours sincerely

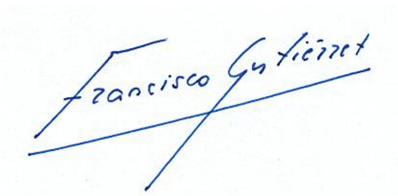

Prof. Francisco Gutiérrez
Editorial Board of Geomorphology
Vice-President of the Int. Assoc. of Geomorphologists

Potential reviewers

Amos Frumkin, msamos@mscc.huji.ac.il, extensive experience on active diapirs, Israel

Mehdi Zarei, zareim@shirazu.ac.ir, extensive experience on active diapirs, Israel

Jiri Bruthans, bruthans@natur.cuni.cz, extensive experience on active diapirs, Zagros Mountains

Highlights

Geomorphic record of diapiric activity (diapiric geomorphology)

Salt flow enhanced by erosional unloading

Impact of active diapirism on drainage network development

Long-term rates of diapiric uplift

Abstract

The structural and stratigraphic features associated with salt structures have received extensive attention. However, there is limited work on the geomorphic and Quaternary record of diapiric activity despite its practical implications (e.g., salt and hydrocarbon extraction, geostorage activities). This work analyses the Quaternary geomorphic and stratigraphic evidence of diapiric activity in the Navarrés salt wall (SE Spain), developed along the axis of a Neogene graben. This salt system is located in a region characterized by a peculiar network of orthogonal grabens that control the drainage network. The protruding salt walls are spatially associated with the erosionally unloaded and deeply entrenched graben sections situated close to the regional base level. Evidence of recent/current activity in the Navarrés salt wall include: (1) internally drained areas in a marginal withdrawal basin with long-sustained Quaternary deposition; (2) distorted drainage network (defeated and deflected streams, wind gaps, knickpoints, changes in fluvial style), which changed from an initial axial longitudinal pattern to a longitudinal marginal distribution at the flanks of the salt wall; (3) development of diapiric fault scarps at the edge of the salt wall; (4) tilted terraces dipping away from the salt wall and locally thickened. The available data indicate along-strike variability in the deformation style and long-term vertical deformation rates. These range from ≤0.09 mm/yr, to significantly higher values (>0.2-0.4 mm/yr) in the section where the salt wall displays a more prominent relief and is affected by deep fluvial entrenchment. The regional analysis and the characterization of the Navarrés salt wall suggest that active diapirism in the region is enhanced by erosional unloading related to fluvial entrenchment, which expands from the regional base level through the upstream propagation of an incision wave.

Geomorphic and stratigraphic evidence of Quaternary diapiric activity enhanced by fluvial incision. Navarrés salt wall and graben system, SE Spain

Francisco Gutiérrez (1)*, Jorge Sevil (1), Pablo Silva (2), Eduard Roca (3), Frederic Escosa (3)

(1) Department of Earth Sciences, University of Zaragoza, Zaragoza, Spain
(2) Department of Geology, University of Salamanca, Salamanca, Spain
(3) Department of Geodynamics and Geophysics, University of Barcelona, Barcelona, Spain

* Corresponding author e-mail: fgutier@unizar.es

Abstract

The structural and stratigraphic features associated with salt structures have received extensive attention. However, there is limited work on the geomorphic and Quaternary record of diapiric activity despite its practical implications (e.g., salt and hydrocarbon extraction, geostorage activities). This work analyses the Quaternary geomorphic and stratigraphic evidence of diapiric activity in the Navarrés salt wall (SE Spain), developed along the axis of a Neogene graben. This salt system is located in a region characterized by a peculiar network of orthogonal grabens that control the drainage network. The protruding salt walls are spatially associated with the erosionally unloaded and deeply entrenched graben sections situated close to the regional base level. Evidence of recent/current activity in the Navarrés salt wall include: (1) internally drained areas in a marginal withdrawal basin with long-sustained Quaternary deposition; (2) distorted drainage network (defeated and deflected streams, wind gaps, knickpoints, changes in fluvial style), which changed from an initial axial longitudinal pattern to a longitudinal marginal distribution at the flanks of the salt wall; (3) development of diapiric fault scarps at the edge of the salt wall; (4) tilted terraces dipping away from the salt wall and locally thickened. The available data indicate along-strike variability in the deformation style and long-term vertical deformation rates. These range from ≤0.09 mm/yr, to significantly higher values (>0.2-0.4 mm/yr) in the section where the salt wall displays a more prominent relief and is affected by deep fluvial entrenchment. The regional analysis and the characterization of the Navarrés salt wall suggest that active diapirism in the region is enhanced by erosional unloading related to fluvial entrenchment, which expands from the regional base level through the upstream propagation of an incision wave.

Key words

Salt tectonics, erosional unloading, diapiric geomorphology, deformation rates, gravitational faulting

1. Introduction

Salt readily flows by viscous deformation (creep) due to its mechanical weakness and negligible yield strength (Jackson and Hudec, 2017). Salt bodies can be extremely mobile and flow vertically and laterally towards areas of lower load, both in the subsurface and at the surface. The movement of salt induces deformation at the ground surface; subsidence and uplift in withdrawal/deflation and accumulation/inflation zones, respectively, and horizontal displacement in areas with lateral flow (e.g., rock spreading). Salt flowage may be driven by two mechanisms that may operate in combination (e.g. Jackson and Talbot, 1986; Warren, 2016; Hudec and Jackson, 2007): (1) buoyancy related to density inversion where light salt is overlain by denser overburden; and (2) differential loading. It is widely accepted that the latter mechanism is the main driver for salt migration and diapirism. Differential loading may be induced by lateral tectonic deformation and gravitational forces. Lateral deviatoric stresses may contribute to compress or stretch salt bodies. Gravitational loading is typically related to elevation changes in the top-salt topography and lateral variations in the weight of the overburden. Lateral load gradients may be associated with prograding sediment wedges (e.g., Ge et al., 1997), ice-sheet loading (Sirocko et al., 2002; Lang et al., 2014) and the excavation of erosional depressions by various processes. For instance, Lang et al. (2014) demonstrate by finite-element modelling that salt structures respond to ice sheet loading and unloading by (1) diapir rise when the ice sheet advances close to the diapir (differential loading) and when the ice retreats (unloading); and (2) diapir fall when the ice sheet covers the diapir. Their model results stress the importance of the limited duration of the glacial loading phases, compared with other differential loading processes such as progradation of sediment wedges or fluvial entrenchment.

A considerable number of works document active salt flowage related to erosion-induced differential loading. The salt tends to flow towards areas unloaded by erosion (e.g., fluvial valleys, erosional depressions). Table 1 presents a review of case studies that illustrate erosion-induced active salt flow from the Colorado Plateau, the Southern Rocky Mountains, the Gulf of Mexico, the Zagros Mountains, the Ebro Cenozoic Basin and the Pyrenees. The table indicates the geological setting, the reported geomorphic and stratigraphic evidence of activity, the local relief between the bottom and margins of the erosional depressions, ranging from 750 to 100 m, and surface displacement rates where available. The impact of erosion on the activation of salt systems is generally considered to be a local factor. Nonetheless, Barnhart and Loman (2012), based on orogen-wide DInSAR data over the Zagros Mountains, observe that the active diapirs are associated with anticlines in which the level of erosion has reached old formations (i.e., Eocene Asmari Limestone or older), suggesting that erosion controls the activation of diapirs at a regional scale.

There is extensive literature dealing with the structural and stratigraphic features associated with active and inactive salt structures developed in a wide range of geological environments (Hudec and Jackson, 2011 and references therein). In contrasts, the investigations dealing with the identification and assessment of diapiric activity recorded by Quaternary landforms and deposits are comparatively very limited, despite the relevant practical implications for safe salt mining, hydrocarbon extraction and geostorage activities (e.g., Köthe et al., 2007). This implies that there is extensive room for innovation in the field of “diapiric geomorphology”, which can be defined as the analysis of the impact of diapiric activity on earth-surface processes, landform development and landscape evolution. The geomorphic responses to the activity of salt structures can be classified into primary effects, related to surface deformation, and secondary effects, comprising various geomorphic processes and features induced by ground deformation.

The main primary effects include the formation of rising elevated areas by upward salt flow (e.g., Martin and Bouma, 1981; Erol, 1989; Autin, 2002) and the development of subsiding depressions by salt withdrawal that may function as traps for sediments (e.g., Martin and Bouma, 1981; Colman, 1993). Extruding salt plugs like those developed in the semiarid Zagros Mountains may produce dome-shaped mountains more than 1.5 km in local relief (e.g., Talbot and Alavi, 1996). When the salt domes reach a critical weight, the load may exceed the yield strength of the salt, so that their lower slopes spread laterally to form salt glaciers (namakiers) (Gutiérrez and Gutiérrez, 2016). Jahani et al. (2007) propose an evolutionary morphologic classification for the salt diapirs in the Eastern Fars Province of the Zagros Mountains: (1) circular domes above buried salt; (2) high-relief salt extrusions; (3) salt extrusions with salt glaciers and a fountain or summit dome above the feeding vent; (4) empty craters with insoluble residues. Diapiric rise, typically with marked spatial gradients, may be recorded by uplifted, upwarped and tilted geomorphic and stratigraphic markers such as fluvial terraces (Kirkham et al., 2002; Jochems and Pederson, 2015; Lucha et al., 2008a, b, 2012; Gutiérrez et al., 2015), marine terraces (Bruthans et al., 2010) or sea-floor deposits (Lee et al., 1996).

Recently, Jochems and Pederson (2015) documented and OSL-dated deformed strath and fill terraces of the Colorado River in a section near Moab, Utah, where the river traverses perpendicularly several anticlines cored by salt walls of the Paradox salt formation. They identified a reach with thickened and subsided fill terraces (Professor Valley) and a section with uplifted strath terraces showing upstream tilting (Salt-Cache salt wall). They estimated long-term subsidence rates in the former reach of 0.5-0.6 mm/yr. The authors attributed these local deformations to active salt flow towards the core of a salt anticline and ascribed this process to differential unloading caused by rapid canyon incision (ca. 500 m). Diapiric uplift may also cause extension on a brittle overburden resulting in the development of normal fault scarps, fissures, graben depressions and horsts (e.g., Farasan Islands, Saudi Arabia; Almalki et al., 2015).

Secondary effects are mainly related to changes in the drainage network due to active vertical deformation (i.e. uplift and subsidence), including the deflection (e.g., Holford et al., 2007; Gutiérrez and Lizaga, 2016), blockage (e.g., Martin and Bouma, 1981; Colman, 1983; Gutiérrez and Lizaga, 2016) or obliteration of channels (Lee et al., 1996). Rising diapirs may also control the development of multilevel cave passages that form by salt dissolution associated with a relatively stationary water table (Frumkin, 1996; Bruthans et al., 2010). Diapiric activity may also increase the relief and gradient of slopes, favouring the development of subaerial and subaquacueous landslides (e.g., Martin and Bouma, 1981; Popenoe et al., 1993; Tripsanas et al., 2004). The 400 km long Cape Fear submarine landslide, North Carolina, is one of the largest mass movements of the U.S. Atlantic continental margin. Its 50 km long and 120 m high amphitheatre-shaped headwall depression has been intruded by two protruding salt diapirs. Popenoe et al. (1993) proposed that the failure was induced by the rising diapirs, which contributed to weaken the associated sediments and over-steepen the slope. Active salt flow may also result in complex secondary geomorphic effects. Lateral salt flow towards an erosional depression may cause the spreading of the overlying debuttressed brittle rocks, resulting in the development of a graben and horst morphostructure, which may cause the distortion of the pre-existing drainage, expressed through wind gaps and knickpoints (Trudgill, 2002; Gutiérrez et al., 2012; Kravitz et al., 2017).

Some recent works nicely illustrate the use of deformed geomorphic markers dated by various geochronological methods to assess long-term rates of diapiric activity. Frumkin (1996) documented multi-level cave passages in Mount Sedom diapir that record paleo-base levels of erosion and diapir uplift. He estimated long-term uplift rates of ≤6-7 mm/yr over the past 8 ka, based on the relative height of the subhorizontal passages and radiocarbon dates from vegetation remains found in cave deposits. Bruthans et al. (2010) documented the geomorphic record of long-term diapiric rise in the Namakdan salt dome, Qeshm Island, Zagros Mountains, Iran, including perched and uplifted marine terraces, fluvial terraces and cave levels. They were able to quantify uplift rates across the diapir, ranging from 4 mm/yr at 600 m from the diapir edge, to 0.4-0.6 mm/yr in the surrounding encasing rocks (300 m wide fringe affected by dragging). The present-day activity of diapirs has been also satisfactorily characterized using ground-based geodetic methods (Zarei et al., 2012) and DInSAR (Furuya et al., 2007; Aftabi et al., 2010; Barnhart and Lohman, 2012; Refice et al., 2016). Aftabi et al. (2010), using DInSAR surface displacement data, unraveled complex concentric strain patterns in the subcircular Syahoo diapir, Zagros Mountains, Iran, which shows a central bulge (salt fountain) and radially spreading salt sheets (namakiers). They record a non-steady deformation of the salt surface with vertical displacement rates ranging from +51 cm/yr and -80 mm/yr. Interestingly, during short wet periods the central bulge experiences uplift, which deflates during the dry periods, which is counteracted by inflation and enhanced flow in the adjacent namakiers.

The present work has been developed in the framework of a project on the seismic characterization of nuclear power plant sites in Spain, required by the Spanish Consejo de Seguridad Nuclear. This project is aimed at conducting a probabilistic hazard analysis of the Spanish nuclear power plants following a Study Level 3 of the guidance advanced by the Senior Seismic Hazard Analysis Committee (SSHAC Level 3) (guidelines NUREG/CR-6372 and NUREG-2117of the U.S: Nuclear Regulatory Commission). The main aim of the work is to assess the potential activity of the Navarrés salt wall and the faults that bound the associated graben, located at 30-40 km form the Cofrentes Nuclear Power Plant. The diapiric geomorphology of the salt wall and graben system is analysed and new geochronological data is used to estimated long-term deformation rates related to salt flowage. Some previous works suggested that the diapirs are flanked by salt welds and are currently inactive (e.g., Moissenet, 1985; Roca et al., 1996). However, this interpretation is not supported by data from the geomorphic and Quaternary record. The Navarrés Graben and salt wall was selected for this study because of the presence of extensive Quaternary deposits and landforms that can be used as markers to identify and assess recent deformation, either diapiric or tectonic.

2. Geological setting

2.1. Structure and stratigraphy

The investigated area is located in the Caroch Massif region, SE Spain, situated in the southern sector of the Iberian Chain, just north of the outermost zone of the Betic Cordillera (External Prebetics) (Beltrán et al., 1977) (SE corner of Fig. 1). This region is designated as the "fractured Betic foreland" (Santisteban et al., 1990) and the Valencian Domain (Baena and Jerez, 1982). The boundary between these two geological domains can be established by (1) an increase to the SE in the thickness of the Mesozoic and Cenozoic successions; (2) a change in the structural grain, with predominance of ENE-WSW-oriented contractional structures in the External Prebetics, south of Xátiva (Vera and Martín-Algarra, 2004); and (3) the occurrence of significant Neogene marine sediments in the External Prebetics. This boundary is associated with the Jumilla Fault, which separates two markedly different gravimetric domains (Castaño and Carbó, 1995) and marks a sharp change in the structural style (Escosa et al., 2018a). Other authors locate the boundary between the Iberian Chain and the Betics at the northern edge of the Caroch Massif region along a NE directed thrust (Valencia Domain Thrust Front; Roca et al., 2013).

The Iberian Chain is an intraplate Alpine orogen with prevailing NW-SE structural trend generated by the tectonic inversion of Mesozoic extensional basins from late Cretaceous to Early Miocene times (Álvaro et al., 1979). Since the Middle Miocene, the region has been affected by post-orogenic extension and the development of grabens superimposed on the previous contractional structures. The development of these grabens is related to the westward propagation of the crustal extension involved in the development of the offshore Valencia Trough from the late Oligocene (Roca and Guimerà, 1992; Anadón and Moissenet, 1996; Capote et al., 2002; Gutiérrez et al., 2008). The Eastern Prebetics represents the foreland fold and thrust belt of the Betic-Balearic orogen, related to the N-S to NNW-SSE convergence and collision of the Iberian and African plates (De Galdeano, 1990). It consists of an allochtonous wedge of Mesozoic and Cenozoic sedimentary rocks detached above Middle-Late Triassic evaporites and mudstones and mainly deformed in Miocene times, in relation to the convergence between the Iberian and African plates (Vera and Martín-Algarra, 2004). This geological domain includes numerous exposed diapirs of Triassic evaporites, some of them with clear evidence of current activity (e.g., Jumilla, La Rosa, Pinoso; Rodríguez-Estrella, 1983; De Ruig, 1995; Rodríguez-Estrella and Pulido-Bosch, 2010; Martínez del Olmo et al., 2015; Escosa et al., 2018b).

The Caroch Massif region is characterised by a thin-skinned structural style, in which a 1.5-2 km thick suprasalt Jurassic and Cretaceous cover, dominated by shallow platform carbonate rocks, is detached from the subsalt rigid basement (non-exposed Paleozoic and Early Triassic rocks) along salt-bearing Middle-Late Triassic evaporitic rocks (mainly Keuper Facies). The carbonate cover is dominated by a subhorizontal structure, although is locally affected by some folds with prevailing NW-SE trend. The tabular structure and topography of the Caroch Massif region is compartmentalized by a peculiar system of graben depressions up to 40 km long with multiple orientations, frequently orthogonal (Moissenet, 1989; De Ruig, 1995; Martínez del Olmo et al., 2015) (Fig. 1). The basin-bounding normal faults may reach throws in excess of 1000 m (e.g., Rubinat et al., 2013). Some of these grabens include a significant Neogene continental fill and are piereced by elongated diapirs (salt walls) with prominent geomorphic expression along their axes, that split the basins into two half-grabens (e.g. Ayora-Cofrentes, Bicorb-Quesa, Navarrés) (e.g., De Ruig, 1995; Roca et al., 1996). At the edges of the salt wall exposures, the Mesozoic and Miocene sediments typically display steep dips away from the diapiric extrusions and may be even overturned. Other graben depressions lack exposures of Triassic diapiric sediments and do not show significant Neogene fills.

The diapiric evaporitic succession corresponds to the Upper Triassic Keuper facies, with an original thickness of around 600-700 m in the area (Suárez-Alba, 2007). It comprises five lithostratigraphic units from base to top (K1 to K5), described in outcrops (Ortí, 1974, 2004) and in oil-exploration wells such as Carcelén-1, situated 50 km west of Navarrés (Suárez-Alba, 2007). They can be grouped into two evaporitic sections (K1 and K4-K5) with a clastic interval in between (K2-K3). Unit K1 (Jarafuel shales and gypsum, 175 m in Carcelén-1) is the main salt unit including 17 halite intervals. Unit K2 (Manuel sandstone, 150 m in Carcelén-1) is a detrital unit chiefly consisting of sandstone layers and interbedded shales. K3 (Cofrentes shales, 50 m in Carcelén-1) is dominated by brick red shale. K4 (Quesa gypsiferous shales, 200 m in Carcelén-1) is a complex succession comprising shale, halite and anhydrite intervals from base to top. The halite package is around 150 m in Carcelén-1. K5 (Ayora gypsum, 50 m in Carcelén-1) is made up of light coloured anhydrite and shales. Halite has an aggregate thickness of around 325 m in Carcelén-1 well, within an Upper Triassic succession 650 m thick (ca. 50%). The original thickness at the location of some diapirs was probably higher, considering that they may be associated with basement faults that controlled the deposition of thicker Triassic successions in the downthrown block. Halite is not present in the frequent exposures of units K1 and K4, and consequently these units should be interpreted as condensed sequences after the dissolution of halite beds (Gutiérrez et al., 2001). The mass depletion related to halite dissolution in the subsurface necessarily results in the formation of insoluble residues and the subsidence of the overlying sediments, which may complicate the structure of both the Keuper facies and the overburden (e.g., Warren, 2016).

The Caroch Massif is fully covered by the Spanish geological map at 1:50,000 scale, mainly produced in the late 1970s (e.g., Beltrán et al., 1977). However, the grabens and salt walls of this area have been scarcely investigated, with the exception of the Bicorb-Quesa graben and diapir system, which has been the focus of detailed structural and stratigraphic studies (Santisteban et al., 1989, 1993, 1994; Roca et al., 1996, 2006, 2013; Anadón et al., 1995, 1998; Rubinat et al., 2010, 2013). The main features of this structure, with some similarities with the Navarrés graben and salt wall, and whose diapir is connected with that of the Navarrés basin (Fig. 1), are summarised below providing the basis for comparing the two adjacent graben and salt wall systems.

2.2. The adjacent Bicorb-Quesa graben

The Bicorb-Quesa graben is a 24 km long and 2-5 km wide basin with ENE-WSW orientation and significant along strike structural variation (Fig. 1). The western sector of the graben is narrower and less deformed, shows restricted outcrops of Miocene deposits and lacks an exposed diapir. The eastern sector, which is abruptly interrupted by the Navarrés graben, comprises a protruding salt wall exposed along the axis and two flanking half grabens with Miocene continental sediments, Bicorb and Quesa basins on the NNW and SSE sides, respectively. These are syn-diapir growth basins that show the following structural elements: (1) Well-defined outer margins controlled by linear normal faults dipping towards the basin. (2) A more irregular margin associated with the edge of the exposed diapir, where the Mesozoic and Miocene sediments have been upturned and affected by reverse faults and folds verging away from the salt wall. (3) Within the half grabens, the Mesozoic carbonate cover form a series of elongated blocks bounded by normal faults mainly dipping towards the salt wall and with displacements that reach 1.3 km. These normal faults are locally cross-cut by reverse faults directed away from the diapir. (4) The Miocene fill of the Bicorb and Quesa basins show an overall open and asymmetric syncline structure with steepened dips close to the diapir.

The Bicorb basin fill, on the NNW flank of the diapir, consists of ca. 650 m of Middle-Late Miocene sediments with a lower alluvial unit (400 m thick, Middle Miocene) and an upper alluvial-lacustrine unit (250 m thick, Late Miocene). The Middle Miocene Quesa basin fill, up to 510 m thick, is dominated by alluvial fan facies with some intercalations of lacustrine limestone (Anadón et al., 1998). The temporal evolution of the salt evacuation basins (Rubinat et al., 2013) and the associated diapir has been inferred on the basis of cartographic relationships and the geometrical and sedimentological characteristics of the basin fills. Gypsum sediments and the bipyramidal quartz crystals of diagenetic origin known as “jacintos de Compostela” were used as indicators of diapir emergence. High input of coarse clastics, slumps and paleolandslides were attributed to relief rejuvenation by normal faulting and diapiric extrusion. Three main phases were inferred with suspected along-strike asynchronicity (Roca et al., 1996; Anadón et al., 1998): (1) First extensional phase (Lower Miocene-Langhian) coeval to the sedimentation of most of the lower unit of the Bicorb basin during which the diapir rose for the first time. (2) Contractional phase (Serravallian) recorded by the development of folds and reverse faults, during which the southern margin of the graben was partially emplaced onto the northern margin, resulting in the closure of the diapir. (3) Second extensional phase (Tortonian) with reactivation of the diapir and the normal faults. In the two dipiric phases, the salt wall went through the typical evolutionary stages of salt structures induced by thin-skinned tectonics, ultimately emerging at the surface (Vendeville and Jackson, 1992): (a) Reactive stage, in which the salt fills the space created the faulted overburden. (b) Active stage, when the salt lifts, pierces and shoulders aside the thinned overburden, which is upturned, dragged and rotated outwards. (c) Passive stage with emergence at the surface and extrusion of the salt wall. Rubinat et al. (2010, 2013), based on detailed mapping and a magnetotelluric survey across the Bicorb-Quesa graben recognised a down-to-the-NNW basement extensional fault beneath the asymmetric diapir with a throw of around 1 km, consistent with the thicker Mesozoic succession on the northern margin of the graben. They also inferred that most of the salt coring the Bicorb-Quesa salt wall corresponds to the lower salt-bearing unit of the Keuper facies (K1). Roca et al. (2013) identified two salt bulbs in the salt wall (two longitudinal double-plunging antiforms) and on the basis of a paleomagnetic study and interpreted that the formation of the Bicorb-Quesa and Navarrés salt walls is related to the southward extensional displacement and clockwise rotation of the cover block located to the south, consistently with the widening of the salt walls to the east and south, respectively.

2.3. Seismotectonics

The Caroch Massif, on the western margin of the Valencia Trough, is characterized by very limited seismic activity over the historical and instrumental periods, especially when compared with adjacent areas to the S and SE associated with the Betic Cordillera (Olivera et al., 1992; Martínez-Solares and Mezcua, 2002). Some EMS intensity ≥VIII earthquakes have been recorded to the south and east of the Navarrés graben: 1396 Tavernes de Valldigna (I= VIII-IX); 1644 Muro de Alcoy (I=VIII); 1748 Estubeny or Montesa earthquake (I=IX). The 1748 Estubeny seismic series, with the largest event on 23rd March, caused severe damage in the region, including large destruction in Játiva town (ca. 6000 inhabitants) and the collapse of the Montesa castle-monastery, resulting in 38 fatalities, of which 22 occurred in the castle (Alberola, 1999). Giner-Robles et al. (2014) and Silva et al. (2014) analysed the geological and archaeological effects of the earthquake using the ESI-07 macroseismic scale (Michetti et al., 2007). They locate the maximum intensity (I=IX, ESI-07) in the Sellent valley, around Estubeny and Sellent villages, and include the Navarrés graben within the I=VII-VIII (ESI-07) intensity zone. Buforn et al. (2015) have recently re-evaluated the focal parameters and modelled the rupture source using macroseismic and geological data. These authors locate the epicenter around 1 km south on Anna and Estubeny (39.00°N 0.64°W), in the southernmost sector of the Navarrés graben, where intensity and acceleration (PGA) reached IX (EMS-1998) and 0.57g, respectively. The proposed rupture model obtained from the spatial distribution of estimated accelerations suggest an 8 km long, NE-SW oriented and SE dipping fault. The limited available earthquake focal mechanisms indicate that the Navarrés salt wall and graben system is located in a transition zone between NW-SE compression to the SE, in the External Prebetics, and dominant NE-SW extension in the Mediterranean fringe and the Betic foreland (e.g., Stich et al., 2018).

3. Methods

Geological-geomorphological mapping was carried out through the interpretation of aerial photographs, orthoimages and shaded relief models derived from digital elevation models with 5 m and 1 m horizontal resolution. Detailed field surveys were carried out in the region to check and refine the preliminary maps produced with remote-sensed data. A hand-held GPS (horizontal accuracy ~3 m) was used to locate key outcrops and sampling points.

A total of ten samples of deformed tufa deposits were collected for U-series dating. Three samples were discarded upon close inspection in the laboratory, due to clear evidence of significant alteration, including dissolution features and precipitation of secondary carbonate, overall suggestive of open system conditions. The analyzed subsamples were extracted using a micro-drill with a tungsten carbide tip. The isotopic measurements were carried out with a Multicollector Inductively Coupled Plasma Mass Spectrometer (MC ICP-MS, Thermo Scientific Neptune) at the Geochronology Facility of CENIEH (Burgos, Spain). A total of 120 measurements were carried out to obtain the isotopic ratios 234U/238U, 235U/238U, 236U/238U, 229Th/232Th, 130Th/232Th by the standard bracketing method with errors below

5%. The concentration of 238U and 232Th was carried out by the isotopic dilution mass spectrometry (IDMS) method. Age estimates have been derived using the general equation of radioactive decay (Cheng et al., 2013) and corrected following the approach proposed by Ivanovich and Harmon (1992) (Table 2). Since the tufa samples cannot be considered perfectly closed systems, the obtained corrected ages should be considered as rough or minimum age estimates for the sampled carbonate deposits. Consequently, the deformation rates derived from them are reported as maximum values.

Samples for Optically Stimulated Luminescence (OSL) dating were collected from fluvial deposits preventing exposure to light by using opaque PVC tubes, or filling light-proof bags with a driller under an opaque tarp. The Gamma dose rate was measured in situ (CANBERRA portable gamma spectrometer with an InSpector 1000 analyzer), and bulk sediment samples were collected from around the sampling point for additional dose rate and moisture-content estimates. The total dose rate was estimated combining the dose of the main radiations (Beta, Gamma and Cosmic) and radioelements (^{238}U, ^{232}Th, ^{40}K) (Table 3). Cosmic dose rate was estimated using correction parameters proposed by Prescott and Hutton (1994). The water content was assumed to be 60% of the maximum saturation value measured in the laboratory with an additional error of 10%. The equivalent dose (D_E) was measured by the Single Aliquot Regenerative Dose (SAR-protocol) on multiple quartz grains using a RISḊO TL/OSL DA-20 (or DA-20 C/D) reader equipped with a $^{90}Sr/^{90}Y$ irradiation source and an approximate dose of 0.10 Gy/s. Quartz stimulation was carried out by blue light (470 nm wavelength and 109 mW maximum power). A central age model (CAM) was applied for samples with overdispersion values below 20% and a minimum age model (MAM) for those with higher values (Galbraith and Roberts, 2012; López et al., 2018). Importantly, the latter ages should be considered as minimum age estimates for the time of sediment accumulation, and consequently yield maximum deformation rates.

4. General morpho-structural features of the grabens and salt walls

The general morpho-structure of the Caroch Massif region is characterised by a complex system of Neogene graben-depressions with orthogonal orientations and intervening plateaus (*muelas*), mainly underlain by Cretaceous carbonate rocks with subhorizontal structure (De Ruig, 1995; Martínez del Olmo et al., 2015) (Fig. 1). Some grabens include a Miocene or Mio-Pliocene continental fill hundreds of meters thick and are pierced by a salt wall of Triassic evaporites along their axes. Other grabens lack salt wall, have a thin Neogene fill, and may display a marked topographic relief, resembling starved basins. The Jucar River, which flows along the northern and eastern sectors of the Caroch Massif, is the regional base level. The trajectory of this drainage, which crosses the Ayora-Cofrentes graben, is controlled by the Júcar, Cortes de Pallás and Tous grabens, from west to east (Fig. 1). The Cabriel River flows along the Cabriel Basin, north of the Caroch Massif region, and joins the Jucar River in the northern sector of the Ayora-Cofrentes graben. The distribution of the main tributary drainages is also controlled by the orthogonal grabens, showing an overall trellis pattern. In the northern and eastern sectors, in association with the main base level (Júcar River), the drainage network is typically deeply entrenched into the Mesozoic and Cenozoic bedrock, locally forming striking canyons. In the areas more distant from the Júcar River, mainly in the southwest sector, the main streams flow along broad and non-dissected graben floors, which locally show poorly-drained zones and desiccated lakes. These grabens are perched and apparently relict tectonic depressions dominated by gently sloping pediments with a restricted and poorly integrated drainage net. The change between deeply entrenched areas and the poorly dissected depressions is generally marked by well-defined knickpoints in the longitudinal profile of the main drainages. These points mark the limits of the areas affected by the headward expansion of fluvial incision.

The region can be divided into two domains separated by the N-S trending Ayora-Cofrentes graben and with different morpho-structural features (Fig. 1). West of the Ayora-Cofrentes graben, the Jurassic-Cretaceous carbonate cover is compartmentalized by an orthogonal system of intersecting E-W and N-S trending grabens. East of the Ayora-Cofrentes depression, the grabens show prevailing ENE-WSW and NNW-SSE orthogonal trends, and the carbonate Mesozoic suprasalt strata shows a gentle regional dip to the northeast that controls the drainage network. Table 4 presents some structural, stratigraphic and topographic features of the different grabens, including the local relief of the depressions and that of the outcrops of diapiric rocks (salt ridges), as rough indicators of the amount of differential topographic loading and the relief created by salt flow.

The E-W trending Júcar and Carcelén grabens are developed along the crest of open anticlines. Cretaceous rocks at the margins of these depressions dip away from the grabens and form well-defined linear scarps. Interestingly, these grabens are controlled by scissor-like normal faults with throws that progressively decrease to the west, away from the Ayora-Cofrentes graben and salt wall (Moissenet, 1985). The 26 km-long Júcar Graben is deeply entrenched by the longitudinal Júcar River canyon and has a Mio-Pliocene sedimentary fill that reaches the Early Pleistocene in its western sector (biostratigraphic zone MN17; Alcalá et al., 1985). The 32 km long Carcelén Graben is a poorly dissected basin that intersects the northern sector of the N-S trending Alpera Graben. Its Neogene fill is largely concealed by Quaternary mantled pediments. It shows an undissected and poorly drained area in the central sector. To the west, the Charco Stream traverses the northern fault scarp through a water gap close to the fault tip. To the east, the poorly entrenched Agua Stream shows an abrupt knickpoint at the eastern edge of the depression, changing into a deeply incised bedrock channel. Las Rochas Graben is also drained by a non-entrenched axial drainage developed on active alluvial surfaces. This basin, developed along the crest of an anticline, is bounded by normal faults with subdued geomorphic expression and has a poorly exposed Neogene fill. The 46 km long and N-S striking Alpera Graben widens to the south and shows a more complex geometry. It intersects the Carcelén Graben and shows minor transverse grabens on the eastern margin. This non-entrenched basin has a poorly exposed Mio-Pliocene fill, interrupted in the southern sector by a bevelled anticline cored by Triassic units older than the Keuper Facies (Quintero et al., 1978; Sopeña et al., 1990). This seems to be a fold detached along a Middle Triassic claystone and anhydrite unit (Röt facies), rather than a diapir. This portion of the graben, far away from the base level, shows poorly-drained areas. The shallow axial alluvial channel (Vega Stream) changes into an entrenched bedrock channel (Zarra Stream) downstream of a knickpoint close to the western margin of the Ayora-Cofrentes Graben, flowing along a secondary cross graben.

The 46 km-long and N-S oriented Ayora-Cofrentes Graben can be divided into two sectors with different features. North of Ayora, it is a deeply entrenched graben by the transverse Júcar River and the longitudinal Jarafuel Stream, and has a prominent salt wall. The elongated diapir splits the basin into two growth half grabens with a Mio-Pliocene fill ca. 300 m thick dominated by alluvial facies (Beltrán et al., 1977). On the western sector, the Neogene succession is capped by a Pliocene limestone (Alcalá et al., 1985; Mazo, 1997) that forms elongated mesas around 300 m above the Júcar River. This limestone unit and the correlative marginal detrital facies overlap the western master fault and penetrates into the Júcar Graben (Beltrán et al., 1977; Santisteban et al., 1990). Southwest of Cofrentes, the Pliocene limestone is downdropped and backtilted by an east-dipping intrabasinal fault system spatially associated with the Keuper Facies (Beltrán et al., 1977; Ortí, 1990). Carner (2001), considering a vertical offset of 120 m and time spans of 5.3 Ma and 3.6 Ma (base of the Pliocene and Early-Late Pliocene boundary), estimated long-term vertical slip rates of 0.022 and 0.03 mm/yr, respectively. In Cofrentes village and its vicinity, there are three main outcrops of Pleistocene alkaline volcanic rocks associated with the junction of the Júcar and Cabriel valleys and derived from the asthenospheric mantle (Martí et al., 1992; Ancochea and Huertas, 2002; Seghedi et al., 2002). Sáez-Ridruejo and López-Marinas (1975) dated by K/Ar the volcanic rocks of the Agrás volcano in two laboratories, providing ages of 2.6-1.8 Ma and 3.9-0.95 Ma. In the vicinity of Cofrentes there is a permanent CO_2-rich bubbling spring of warm water (Los Hervideros). According to Pérez et al. (1996), the $^3He/^4He$ ratio of 0.95Ra (Ra represents the ratio of the helium isotopes in the atmosphere) indicates a mantle-sourced helium fraction of 12% that ascends through a deep basement fault. To the south of Ayora, most of the graben floor is mantled by poorly dissected Quaternary alluvium, interrupted along the axis by inliers of Triassic evaporites and deformed Neogene detrital deposits. In the southernmost sector, north of Almansa, the bottom of the basin remains as an internally drained area with mantled pediments that grade into a large desiccated lake locally known as La Laguna (Lendínez and Tena, 1978).

The salt wall of the Ayora-Cofrentes graben connects with the E-W trending salt walls associated with the Cabriel River and the Cortes de Pallás Graben. The latter is a 15 km-long and NNE-SSW oriented graben deeply incised by the Jucar River. It has a broad and prominent salt wall and shows limited outcrops of Neogene sediments, most probably due to extensive erosion. Interestingly, the Jucar River, rather than flowing along the easily erodible Triassic evaporites, it has excavated a deep and narrow canyon in the more resistant Cretaceous limestones on the SE side of the diapir. The Sácaras Graben is a deep and flat-floored trough perched above the adjacent base levels (250 m above the Júcar River). It is essentially a half-graben controlled by a main fault on the NE side, that controls a prominent escarpment with upturned Cretaceous rocks in the footwall (Roca et al., 2013). The graben connects with the Cortes de Pallás and Bicorb-Quesa grabens to the north and south, respectively. Its bottom displays a poorly drained area and shallow longitudinal drainages that flow towards the adjacent grabens. The Bicorb-Quesa Graben, described above, is deeply entrenched and is mainly drained by longitudinal streams connected to the Escalona River. The Navarrés Graben, which is described below in detail, hosts a prominent axial salt wall with poorly drained marginal depressions underlain by Neogene sediments, largely concealed by Quaternary deposits. The narrow NNW-SSE-trending Tous Graben controls the path of the Júcar River and lacks both Neogene sediments and salt wall. The topography of this graben may be largely related to structurally controlled erosion associated with the incision of the Júcar River. West of the Navarrés Graben there are some additional ENE-WSW unnamed graben depressions with longitudinal drainages with rather subdued geomorphic expression.

The general morpho-structural analysis indicates that fluvial incision in the region has propagated southwards and westwards from the Júcar River, mainly through headward migration of knickpoints in longitudinal drainages controlled by grabens. This long-term incision wave has determined a time-transgressive change in the morpho-sedimentary behaviour of the grabens, from aggradational to incisional, like in other regions of the Iberian Chain (Gutiérrez et al., 2008). The younger sediments of the Bicorb-Quesa graben are Late Miocene in age (Anadón et al., 1998), the sedimentary fill of the Cofrentes-Ayora graben, further away from the Mediterranean coast, reaches the Pliocene (Alcalá et al., 1985; Mazo, 1997), whereas the youngest sediments in the western sector of the Júcar Graben are Early Pleistoicene in age (Alcalá et al., 1985). Upstream of the areas affected by fluvial entrenchment, the grabens remain undissected, showing flat, alluviated floors and poorly- or internally-drained areas.

The hydrogeology of the Caroch Massif is mainly determined by (1) the presence of extensive plateaus underlain by permeable carbonate rocks that function as important recharge areas; (2) a general topographic drop towards the east; and (3) the presence of salt walls that act as hydrogeological barriers, dividing the region into different subsystems. East of the Ayora-Cofrentes Graben, the connected salt walls of Bicorb-Quesa and Navarrés separate the Northern Caroch and Southern Caroch hydrogeological subsystems (Fig. 1). In the Southern Caroch, the regional groundwater flow is directed towards the western margin of the Navarrés Graben, where the main springs are located (Anna and Las Fuentes or Playamonte). The spring waters, with low ionic content (250-400 mg/l), are characterised by a calcium bicarbonate composition (IGME, 1989). These features suggest that regional groundwater flows do not interact significantly with the Navarrés diapir and support the idea that deep-seated salt dissolution has a limited impact on the Navarrés salt wall (e.g., dissolution-induced collapse).

5. The Navarrés Graben

5.1. Structure and stratigraphy

The NNW-SSE-oriented Navarrés salt wall and graben system, controlled by extensional faults on both margins, is 20 km long and reaches 4.3 km in width on its central sector (Fig. 2). The graben and the salt wall connect in its northern sector with the Quesa Half-graben and the adjoining Bicorb-Quesa salt wall (Fig. 1). The margins of the graben are underlain by Jurassic and Cretaceous formations dominated by carbonate sediments with a gentle NE regional dip (Figs. 2, 3). Geomorphologically, these are gently sloping structural surfaces concordant with the underlying structure. The western margin is dissected by down-dip streams that drain large catchments, whereas the drainage basins on the east margin, carved by anti-dip streams, have a very restricted catchment area. This drainage asymmetry has influenced both the infill of the basin and its geomorphic evolution.

The Western Fault of the graben has a well-defined 12 km long trace. It functions as a hydrogeological barrier, controlling the location of majors springs (Navarrés, Las Fuentes, Anna) that drain the regional Southern Caroch karst aquifer system (IGME, 1989) (Fig. 2). The 16 km long Eastern Fault shows in its southern sector two right-stepping and overlapping segments and an associated, partially exhumed, relay ramp. The Cretaceous strata in the footwall are abruptly flexed up along a narrow band next to the faults, showing dip reversals on the western margin and over-steepened dips on the eastern margin (Fig. 3). This feature, also documented in the Bicorb-Quesa Graben (Roca et al., 2013), is attributed to salt inflation in the footwall of suprasalt faults developed above reactive diapirs (i.e., salt rollers) (Vendeville and Jackson, 1992a). On both margins of the graben, the master Western and Eastern faults cross-cut a series of apparently older normal faults and grabens.

The Navarrés Graben is pierced along its axis by a protruding salt wall of Triassic evaporites (Keuper facies) that splits the basin into two half grabens (Figs. 2, 3). The active rise of the diapir has rotated upwards and outwards the adjacent Cretaceous and Neogene thinned succession. The outcrops of Cretaceous rocks abutting the diapiric extrusion form prominent strike-parallel ridges in which the upturned strata show nearly vertical attitude and are locally overturned. Some of these outcrops of Cretaceous limestone were incorrectly mapped as dolomitic Middle Triassic Muschelkalk facies by Beltrán et al. (1977). In some outcrops, the Cretaceous limestones next to the diapiric contact are brecciated and show shear banding. The continental Neogene sediments in the Eastern and Western half-grabens are poorly exposed due to limited fluvial dissection. They consist of massive, strongly cemented, calcareous breccias close to the graben-bounding faults, that grade into orange sandstone and siltstone beds with interlayered subrounded conglomerates. Interbedded layers of tufaceous limestone have been identified at restricted outcrops in the Western Basin. Beltrán et al. (1977) ascribed a Middle-Late Miocene age to the Neogene sediments of the Navarrés Graben, most probably based on biostratigraphic data from the adjacent Bicorb-Quesa Graben. In both basins, the exposed Neogene sediments show asymmetric synclinal structures (Fig. 3). Next to the diapir, the Neogene sediments, shouldered aside during the active rise of the diapir, show steep outward dips. The dip of the strata rapidly attenuates away from the salt wall, attaining a general gentle basinward dip.

The NNW-SSE trending Navarrés salt wall connects with the ENE-WSW oriented Bicorb-Quesa and Sellent salt walls on its northern and southern sectors, respectively, forming a continuous crank-shaped salt structure (**Fig. 1**). The Navarrés diapiric extrusion shows a general southward widening and reaches a maximum span of 2 km around Chella and the transverse Bolbaite Creek, where it shows the highest overall relief. Roca et al. (2013) mapped the internal structure of the northern sector Navarrés salt wall, consisting of tight subvertical folds, and interpreted that the Navarrés Graben and salt wall are controlled by a NNW-SSE-oriented and ENE-dipping basement fault with a throw of around 800 m. These authors, based on a paleomagnetic study, inferred that the formation of the Bicorb-Quesa and Navarrés salt walls in the Late Miocene was influenced by southward extensional displacement and clockwise rotation of the overburden block located to the southwest. This kinematic model is consistent with the widening of the Bicorb-Quesa and Navarrés salt walls to the east and south, respectively. Evidence of dissolution-induced subsidence in the salt wall is restricted to a few highly degraded sinkholes north and south of Bolbaite Creek (Fig. 1).

5.2. Morpho-stratigraphic sequence

The Navarrés Graben has a poorly integrated drainage network that has experienced a complex evolution. The paleodrainages and the currently existing streams have developed stepped terrace sequences that are used in this work as markers to identify and assess potential recent tectonic and diapiric deformation. All the mapped terraces in the area consist of resistant tufa deposits, except for the detrital terraces formed by the Bolbaite Creek within the salt wall (Fig. 2). The light coloured tufa deposits show the typical fluviatile facies, with abundant oncoids, encrusted phytoclasts, intraclasts and micritic tufa, as well as subordinate autochthonous deposits such as small phytoherms and stromatolitic lamination (Pedley, 1990). The clastic terraces of the Bolbaite Creek are characterized by well-rounded and well-sorted gravels and abundant fine-grained facies.

The uppermost morpho-stratigraphic level corresponds to a series of tufa terraces (labelled as T in figure 2) capping the outcropping Navarrés salt wall. These are elongated terrace remnants parallel to the strike of the salt wall that record an old axial drainage. The top of these deposits shows a wide range of elevations between 289 and 351 m a.s.l., which may be related to differential diapiric uplift. This tufa deposits could be early Pleistocene or even late Pliocene in age. The rest of the terraces are inset with respect to this terrace and the crest of the diapir ridge.

The drainage network in the Navarrés Graben shows two domains with different base levels (Fig. 2). The transverse and deeply entrenched Escalona River acts as the base level for the northern sector. East of the salt wall, the longitudinal Insa and Charcos creeks are entrenched into the Neogene fill of the Eastern Basin and into the Cretaceous rocks of the graben margin, respectively. The West Creek is carved into the Neogene sediments of the Western Basin and the Triassic evaporites of the salt wall. In the mapped area (Fig. 2), we have differentiated three terrace levels of the Insa Creek (Ti1: +130 m; Ti2: +85 m; Ti3: +65 m) and two terrace levels of the Escalona River (Te1: +65 m; Te2: +50 m). Terraces Ti3 and Te1 are correlative. The relative height of some terraces may change substantially due to vertical deformation and the non-graded longitudinal profile of some drainages, locally with high-relief knickpoints. A quarry excavated in a tilted tufa terrace deposit (geographical coordinates 30S 698721/4332248) ascribed to terrace Ti1 displays soft sediment deformation structures (e.g., convolute bedding, flames) attributable to fluidization processes. Three terrace levels have been mapped on the west side of the salt wall and associated with the West Creek (Tw1; Tw2; Tw3). Terrace Tw3 is perched around 50 m above the West Creek and could be correlative to terrace Te2. Terraces Tw1 and Tw2, discussed below, are perched above a large internally-drained basin developed on the bottom of Western Basin, north of the Bolbaite Creek (Fig. 2).

North of Bolbaite, there are two extensive tufa terraces (Tt1, Tt2) inset with respect to the uppermost terrace. Terrace Tt1 overlaps the eastern edge of the salt wall (Fig. 2). These terraces can be attributed to a paleoBolbaite Creek, when it used to traverse the salt wall in a more northern position than the current one. The tufa deposits capping the Triassic evaporites show a general eastward inclination and the paleocurrent indicators (channels, frontal accretion stratification) point to an east-directed flow.

The Sellent Creek, after the confluence of the Bolbaite and Riajuelo creeks, is the base level of the southern sector of the Navarrés depression (Fig. 2). The Bolbaite Creek flows longitudinally along a transverse graben on the western margin of the Navarrés Graben. In the Western Basin it is a non-entrenched drainage with a sharp southward deflection north of Bolbaite. Then it flows along the ENE edge of the Western Basin and enters the diapir crossing a water gap carved across upturned Cretaceous rocks, where it shows a striking knickpoint and a water fall (Salto de Chella). Downstream, the Bolbaite Creek is deeply entrenched into Triassic evaporites. In this transverse entrenched section, the Bolbaite Creek has generated three levels of detrital terraces (Tb1: +70 m; Tb2: +50-58 m; Tb3: +40 m). The longitudinal Malet Creek has developed two main terrace levels (Tm1: +40 m; Tm2: +15-18 m) and the upper one can be correlated with terrace Tb3. The transverse Riajuelo Creek crosses the Western Basin through a poorly entrenched alluvial channel and changes into a deeply entrenched bedrock channel with an abrupt knickpoint and a water fall (Salto de Anna) at the edge of the salt wall. The terraces of the Riajuelo and Sellent creeks form a sequence of five levels (Ts1: +165 m; Ts2: +140 m; Ts3: +100 m; Ts4: +65-70 m; Ts5: +30 m; relative height with respect to the entrenched sections of the creeks).

6. Assessment of recent tectonic and diapiric activity

6.1. Recency of the graben-bounding faults

Several lines of evidence indicate that the bounding faults that controlled the development of the Navarrés graben have not experienced recent surface displacement. The Western Fault is overlapped on its northern sector by Neogene sediments of the graben fill (Beltrán et al., 1977) (Figs. 2, 3). This fault does not show any geomorphic feature along its whole trace indicative of recent activity, such as fault scarps or triangular facets (Keller and Pinter, 1996; Bull, 2007; Burbank and Anderson, 2012). In contrast, it shows large embayments such as the broad alluvial plain of the Bolbaite Creek (Fig. 2). Similarly, the Eastern Fault lacks any evidence of Quaternary activity. On the left margin of the Escalona River, the fault, which juxtaposes Cretaceous strata against Miocene conglomerates, is truncated by non-deformed deposits of a mantled pediment correlative with the Te2 terrace of the Escalona River, situated at around 50 m above the current channel (Fig. 4). This alluvial level, according to its relative height, can be ascribed to the Middle Pleistocene (Silva et al., 2015). The sinuous Charcos Creek, associated with the Western Fault, mainly flows along the upthrown block and traverses the fault trace at several locations. Activity of the fault would tend to confine the creek to the downthrown block.

6.2. Evidence of active diapirism

The Navarrés salt wall shows multiple structural, stratigraphic and geomorphic evidence of Quaternary, and most probably current diapiric activity. The majority of these features are illustrated in the geomorphological-geological map of figure 2. They are documented below following the chronological order of the deformation markers and by sectors.

The morpho-stratigraphic markers

The elongated remnants of the uppermost tufa terrace, oriented parallel to the salt wall and related to an axial paleodrainage, show significant variations in elevation and clear strike-parallel NNW and SSE post-sedimentary tilting (Fig. 2). These deformations can be attributed to along-strike variations in the long-term uplift of the salt wall and development of local saddles and culminations. For instance, the terrace north of Navarrés is tilted to the NNW, whereas east of Navarrés, the tufa caprock shows an open synformal structure.

In the northern sector, tufa terraces associated with the eastern edge of the salt wall are tilted away from the diapir, like the Miocene and Cretaceous strata, but with lower dips. For instance, terrace Ti1 dips around 20 degrees (Fig. 2). North of Navarrés village, tufa terraces Tw1 and Tw2 are affected by a steep diapiric contact along the western edge of the salt wall (Fig. 5). Terrace Tw1 occurs on both sides of the salt wall edge and has been offset due to vertical diapiric displacement. The deposit of terrace Tw1 is around 12 m thick on the upthrown side (salt wall), whereas it reaches more than 18 m in thickness on the downthrown side (Western Basin), probably related to synsedimentary diapiric activity. The terrace tread has been offset vertically 19 m. A tufa sample (laminated facies; C-NA-SU1) collected 2 m below the terrace surface on the upthrown side has yielded a U/TH age estimate of ≥241±15 ka. This numerical age and the measured throw indicate a rough long-term vertical displacement rate at the western edge of the salt wall of ≤0.07-0.08 mm/yr.

Terrace Tw2, more than 12 m thick, is restricted to the western side of the salt wall and its aggradation surface is inset 8 m below the tread of terrace Tw1 in the downthrown side (Fig. 5). The deposit of terrace Tw2 is more friable and less weathered (lighter color and devoid of large dissolution voids with speleothems) than that of the older terrace Tw1. An exposure of the salt wall edge at point 30S 0698993/4331282 displays a steep contact dipping into the diapir (N146E 70NE) that juxtaposes Triassic sediments (upthrown side) against tufa deposits of terrace Tw2 (Fig. 5C). The contact is defined by a shear zone around 1.5 m wide in the more brittle tufa, and the tufa shows a drag fold that rapidly attenuates away from the diapiric contact, attaining a subhorizontal attitude. This exposure indicates a minimum post-terrace Tw2 vertical displacement of 12 m, given by the vertical distance between the highest and lowest faulted tufa beds observable in the outcrop. Samples collected at 0.5 m (phytoclasts; C-NA-SU4) and 10 m (phytoherm; C-NA-SU5) below the terrace surface have yield U/Th age estimates of ≥140.6±7 and ≥211±10.5 ka, respectively. The minimum throw and the available numerical ages for terrace Tw2 indicate rough vertical displacement rates on the western edge of the salt wall of 0.08-0.09 mm/yr and 0.05-0.06 mm/yr, respectively. A similar outcrop, showing a diapiric contact between subvertical Triassic sediments and drag-folded tufa deposits of terrace Tw2 is found further south at 30S 0699168/4331036 (Fig. 6). Here, the master "reverse fault" (N155E 52NE) is defined by a decimeter-wide shear zone and a sliver of tufa. The tufa on the downthrown side shows secondary reverse faults with lower dip. On the upthrown side, there is a small remnant of tufa. In case it would correspond to the same unit, the vertical distance between the base of the tufa deposit on both sides of the diapir edge would indicate a minimum vertical offset of 10.5 m (base of tufa on the downthrown side is not exposed).

North of Bolbaite, an east-flowing paleotransverse drainage generated two tufa terraces (Tt1, Tt2) (Figs. 2, 7). On the diapir these terraces show a gentle syndepositional eastward inclination. The upper terrace is carved by an E-W oriented, perched and abandoned valley 100-220 m wide (wind gap). The terrace Tt1 is offset vertically ca. 18 m along the western edge of the salt wall. Here, differential vertical displacement has generated a well-preserved diapiric fault scarp underlain by resistant tufa deposits with poorly exposed dilated joints and shear zones. It is quite likely that this scarp is related to creep displacement on a steep diapiric contact, although it is not exposed. On the downthrown side, terrace Tt1 is slightly backtilted towards the fault scarp and is less dissected than the equivalent surface on the upthrown side. Three samples collected from the tufa terrace Tt1 for U/Th dating on the upthrown side at 2.3 m, 2.5 m and 3 m below the terrace tread yielded ages of >149.7±7.4 ka, >186.4±6.2 ka, and >272.3±4.2 ka, respectively. Most probably the oldest age obtained for this tufa terrace is the best approximation to the actual chronology due to two reasons: (1) according to its morpho-stratigraphic position, should be older than the terraces dated in Navarrés, with ages as old as 241 ka; (2) a sampled from a fluvial deposit nested into this terrace has provided a minimum OSL of 176±10 ka (see below). The maximum age obtained from the tufa terrace, together with the cumulative vertical displacement of 18 m related to diapiric activity, indicate a long term vertical displacement rate of ≤0.07 mm/yr.

The wind gap has some remnants of nested fluvial sediments on its western sector. The alluvial fill is exposed in a transverse artificial cutting located at 30S 0700953 / 4327927. This exposure shows 3.1 m of reddish, relatively massive, fine-grained facies with scattered subangular granule-sized reworked tufa clasts. An OSL sample collected 1.9 m below the top of the fluvial sequence has yielded an age estimate of ≥176±10 ka, providing a maximum chronological bound for the abandonment of this paleochannel. The elevation difference between the top of the fluvial deposits in the wind gap (285 m) and the bottom of the adjacent western basin (272 m) of 13 m could be considered a rough estimate of vertical displacement subsequent to the abandonment of the wind gap. These data indicate a vertical displacement rate of ≤0.07-0.08

mm/yr, assuming no erosion or aggradation in the Western Basin and that the uncertainty of the OSL age covers the age of the wind gap abandonment. Terrace Tt2 on the diapiric extrusion is affected by the fault, but it has been eroded in the downthrown side, where a younger terrace of the Malet Creek has been deposited.

On the western side of the salt wall, a 500 m long remnant of terrace Tb2 of the Bolbaite Creek displays evidence of synsedimentary and postsedimentary deformation (Figs. 2, 8). The detrital terrace deposit just downstream of the Chella waterfall reaches more than 50 m in thickness; (i.e., its base is located beneath the valley floor). Downstream, it wedges out and unconformably overlies the Triassic diapiric bedrock. The measured strikes (NNW to NW) and dips (up to 35 SW) indicate that the terrace deposits are rotated away from the salt wall axis. This sedimentary wedge with an overall cumulative wedge-out arrangement (growth unconformity) records synsedimentary differential subsidence at the edge of the diapir. Moreover, the fluvial succession shows a high proportion of fine-grained floodplain facies and includes light grey marls deposited in palustrine environments, probably indicative of temporary drainage ponding related to differential vertical deformation. The terrace surface shows a clear postsedimentary tilt towards the edge of the salt wall. It also shows a slight apparent upstream tilting in the direction of the Bolbaite Creek. Differential postsedimentary vertical displacement along this 500 m long terrace remnant can be roughly estimated at 3-4 m considering the current gradient of the Bolbaite Creek and the topography of the terrace tread. Two samples have been collected for OSL dating in the thickened terrace deposits at 25 m (C-CHE-OSL4) and 40 m (C-CHE-OSL3) below the terrace surface, yielding ages of 164±9 and 138±10 ka (central age model), respectively. The terrace deposits at this site record a differential vertical displacement of 44 m (i.e., synsedimentary subsidence plus postsedimentary tilting) occurred after the deposition of the oldest dated unit. This indicates a differential vertical displacement rate of 0.25-0.28 mm/yr. Downstream, on the eastern flank of the salt wall, terrace Tb3 of the Bolbaite Creek shows an anomalously downstream over-steepened inclination indicating postsedimentary tilting away from the salt wall (Fig. 9). Overall, the terraces of the transverse Bolbaite Creek show a general upwarping across the diapiric extrusion and differential subsidence on the SW edge

The Riajuelo Creek has deposited two morphostratigraphic units in Anna area, on the western flank of the diapir (Fig. 10). These units are exposed in a large quarry SE of Anna village and in the canyon carved by the Riajuelo Creek, which shows an abrupt knickpoint in the Anna waterfall. The lower unit corresponds to tufa terrace Ts4, which unconformably overlies the salt wall and the adjacent conglomerates. It shows evidence of synsedimentary and postsedimentary deformation. The tufa deposit thickens towards the edge of the diapir, from less than 5 m in its distal edge, to more than 50 m downstream of the Anna waterfall. Upstream, the tufa overlying the Miocene conglomerates at the site of the Anna waterfall is 25 m thick. This thickness variations records synsedimentary subsidence along the edge of the salt wall. Moreover, the top of the tufa unit has been rotated away from the diapir axis, showing a minimum elevation difference of 30 m in the Anna quarry (Fig. 10). The upper unit corresponds to the deposits of a low-gradient alluvial fan that unconformably overlies the tilted tufa unit with an offlap relationship. It mainly consists of loose sheet-like beds of reddish sands and silts with some gravels. In Anna quarry, this unit, at least 14 m thick, thickens towards the edge of the diapir. The distal pinch-out of this offlapping unit is controlled by the differential uplift of the underlying tufa unit. This younger unit seems to be affected by a slight postsedimentary outward rotation opposite to its syndepositional dips. These data, consistently with the evidence found in the Chella waterfall area, indicate general uplift of the salt wall and local subsidence along its western edge. A sample collected for U/Th dating from the tufa unit 1 m below its upper contact in the Anna quarry (C-AN-SU1; phytoclasts), yielded an age of ≥79.3±3.9 ka. This numerical age indicates a differential vertical displacement rate of ≤0.36-0.39 mm/yr.

The drainage network

The drainage network in Navarrés Graben shows a number of anomalies attributable to differential vertical deformation related to salt flow, both inflation and deflation. The long-term evolution indicates a change from a longitudinal drainage developed on Triassic evaporites along the axis of the salt wall (uppermost terrace), to marginal longitudinal drainages mainly running along the flanking withdrawal basins, and locally traversing the salt wall from W to E. The rise of the diapir has generated a water divide where a valley floor once stood, eventually functioning as a barrier for transverse drainages.

The Western Basin, which receives the runoff of the largest catchments, shows a 4 km long internally drained area north of the Bolbaite Creek. This enclosed area, perched above the Escalona River, eventually spills towards the West Creek through a tufaceous cascade called Los Chorradores (La Roca et al., 1996). In the southern sector, this basin has a palustrine zone (Marjal de Navarrés) drained artificially. Here, a 25 m deep borehole was drilled for paleoenvironmental investigations, revealing a succession dominated by distal alluvial fan deposits with palustrine facies in the upper 8 m. Six non-calibrated radiocarbon ages from the upper 2.3 m ranged from 20.7 to 3.4 ka. The detrital alluvial facies were dated at depths of 10, 13, and 21 m, yielding ages of 107,000±16,000, 112,000±6,000; 178,000±27,000, respectively (La Roca et al., 1996; Dupré et al., 1998). These data point to long-sustained subsidence in this sector of the Western Basin, ascribable to salt depletion (withdrawal basin). The TL ages consistently indicate long-term aggradation rates of 0.1 mm/yr.

The transverse Bolbaite Creek used to cross the salt wall during deposition of the tufa terraces Tt1 and Tt2 and the development of the associated wind gap. At the present time it shows a sharp southward deflection next to the edge of the salt wall, flows longitudinally along the Western Basin, and traverses the ridge of upturned Cretaceous limestones through a water gap in Chella (Fig. 2). This change in the path of the Bolbaite Creek can be attributed to the combined effect of (1) uplift in the salt wall at higher rate than the incision capability of the fluvial system; and (2) subsidence in the Western Basin. South of Chella, the Western Basin also shows a poorly-drained non-dissected area suggestive of ongoing subsidence.

The Bolbaite Creek traverses the salt wall, showing marked changes in the fluvial style. Upstream of the Chella water fall, the Bolbaite Creek is a poorly incised alluvial-bedrock channel (Fig. 11). Downstream of the knickpoint, it has formed a deeply entrenched canyon in the easily erodible Triassic sediments of the diapir. Here it shows two contrasting sections. Upstream of the topographic axis of the diapir, where differential uplift is expected to reduce the channel gradient and the stream power, the creek shows a rather straight pattern (sinuosity index 1.1). In the downstream section, where diapiric rise causes the steepening of the channel, the creek shows a highly tortuous path (sinuosity index of 2.1). This type of tortuous bedrock channels with highly sinuous ingrown meanders is characteristic of transverse drainages affected by gradient steepening related to differential vertical deformation. The concurrent gradient and stream power increase leads to enhanced incision and lateral migration, creating a longer and less steep channel that is able to counterbalance the stream power excess induced by differential vertical deformation (Harvey, 2007 and references therein).

The drainage in the Eastern Basin, which receives the runoff from smaller catchments, is dominated by longitudinal drainages carved into Miocene sediments; Insua Creek and Malet Creek (Fig. 2). This sector also has a poorly-drained area in the headwaters of the Charcos Creek that has not been integrated in the fluvial net.

The topography

Generally, the easily erodible Upper Triassic Keuper facies tends to occur in the topographically lower areas and are typically concealed by Quaternary alluvium. However, these soft Triassic sediments form a prominent ridge in the Navarrés graben depression. The salt wall reaches the highest elevations in the buttes and mesas where it is capped by the uppermost tufa terraces. The elevations at these points is equivalent to that of the graben margins and around 100 m higher than the floor of the Western Basin. The Navarrés depression has experienced a relief inversion related to the long-term diapiric extrusion. The diapir axis used to be the locus of an axial longitudinal drainage (valley floor), whereas at the present time, the tufa deposits accumulated in the primitive valley form the highest points of the salt wall. The sector of the salt wall with most prominent topographic relief, despite the Triassic sediments are not protected by tufa caprocks, is located NE of Chella (Fig. 2). Topographic and geological evidence, as well as the estimated strain rates indicate that this is the sector of the salt wall affected by more rapid inflation in recent times. It coincides with the area affected by deeper entrenchment and more intense incision, suggesting that the associated erosional unroofing and unloading may have contributed to enhance upward salt flow in this sector.

7. Discussion and conclusions

7.1. Regional morpho-structural features

The investigated region is characterised by a peculiar system of Neogene graben depressions with orthogonal orientations and intervening polygonal fault blocks with a dominant tabular morpho-structure (Moissenet, 1985; de Ruig, 1995) (Fig. 1). Some of those grabens are pierced along their axes by topographically prominent salt walls that split the basins into two flanking half-grabens with Mio-Pliocene continental fills hundreds of meters thick (e.g., Santisteban et al., 1990; Anadón et al., 1998). Martínez del Olmo et al (2015) attribute the multidirectional grain of the extensional post-orogenic basins to the influence played by pre-existing diapirs. Simón (1989), in the central sector of the Iberian Chain, documents secondary faults associated with outcrops Triassic evaporites at right angles to the master basin-bounding Neogene grabens. This author, based on paleostress analyses, fracture patterns and macrostructures, infer a radial extensional stress regime during the Plio-Quaternary, ascribed to a hypothetical crustal doming process. Gaullier and Vendeville (2005), by means of experimental models, tested the generation of orthogonal grabens by radial spreading in sedimentary lobes deposited above mobile salt. Outward radial spreading is accommodated through the development concentric and radial grabens and polygonal fault blocks. However, the investigated region does not fit with this model that explains gravitational deformation in semicircular and laterally unconfined, prograding sedimentary lobes. In some sectors, such as the western margin of the Ayora-Cofrentes Graben, the formation of orthogonal and locally intersecting grabens devoid of salt walls (Júcar, Carcelén, Alpera grabens) could be related to bidirectional spreading of the overburden due to lateral salt flow towards two elongated diapirs with perpendicular orientations; the N-S-oriented salt wall of Ayora-Cofrentes and the E-W-trending salt wall of the Cabriel valley (Fig. 1). This genetic mechanism, involving lateral salt flowage and extension of the brittle suprasalt strata, would be analogous to the origin of the Grabens of Canyonalnds, Utah (Kravitz et al., 2017 and references therein), and the grabens of Peracalç Range, Pyrenees (Gutiérrez et al., 2012). The throw of the faults that control the E-W-oriented Júcar and Carcelén grabens decreases progressively towards their western tip, away from the adjacent N-S-trending Ayora-Cofrentes salt wall (Moissenet, 1985). This scissor-like displacement pattern, instead of the typical bow-shaped geometry, suggests that the movement on these faults may be related to preferential lateral salt-flow along salt-migration paths underlying the grabens. Nonetheless, the multidirectional pattern of the grabens in the Caroch Massif region and its probable relationship with a thick layer of mobile salt remains as an unresolved issue.

The drainage network in the area, with an overall trellis pattern, is largely controlled by the graben depressions with dominant perpendicular orientations (Fig. 1). Most of the grabens are drained by longitudinal streams that ultimately flow towards the deeply entrenched regional base level. This is the Júcar River, whose trajectory is controlled by several grabens along the northern and eastern peripheral sectors of the Caroch Massif. Close to this base level, the drainage network is deeply entrenched into the Mesozoic and Cenozoic bedrock. These are the areas affected by greatest erosional unloading, where the salt walls show the most prominent local relief. In contrast, in the more distant sectors, the graben floors are typically perched alluviated surfaces with non-entrenched axial drainages and poorly-drained areas or paleolakes. Generally, there is a sharp change between the deeply entrenched and poorly dissected depressions, defined by conspicuous knickpoints in major drainages. These steps in the longitudinal profile of the drainages are related to the headward propagation of an incision wave and the associated time-transgressive change from relatively stable to actively incisional landscapes. As explained below in the discussion on the Navarrés graben, differential loading induced by incision may play some role on the dynamics of the salt walls. Moreover, the extrusion of salt walls along the graben axes contributes to modify the initial simple pattern of depressions drained by longitudinal axial drainages.

7.2. Evidence of diapiric activity in the Navarrés graben

There is board consensus among the different authors regarding the genetic link between the regional tectonic extension and the development of salt walls in the Caroch Massif region (Moissenet, 1985; de Ruig, 1995; Roca et al., 1996, 2013; Martínez del Olmo et al., 2015). There is a clear spatial correlation between the salt walls and the main grabens with thick Neogene sedimentary fill. Moreover, geophysical investigations carried out in the Bicorb-Quesa graben and salt wall revealed a spatial association between these structures and extensional faults in the basement with hectometre-scale throws that controlled the Mesozoic sedimentation and changes in the thickness of the salt layer (Rubinat et al., 2010, 2013). Nonetheless, data on the potential current activity of the diapirs is lacking. This is mainly related to the limited attention paid to the Quaternary geology and geomorphology of the grabens and associated salt walls. Moissenet (1985) indicated that diapiric activity ceased in the area by the end of the Neogene. The evolutionary models proposed for the Bicorb-Quesa graben and salt system implicitly suggest that diapirism stopped in the Late Miocene (Roca et al., 1996; Rubinat et al., 2013). Roca et al. (1996) indicated that the uppermost Late Miocene conglomerates of the Bicorb basin overlap and truncate the graben-bounding normal faults, "indicating the cessation of faulting and probably the end of the rise of the Bicorb-Quesa diapir". Geological cross-sections across the Navarrés Graben propose the presence of salt welds at the margins of the salt wall (Roca et al., 2013). However, the work carried out in the Navarrés Graben, largely focused on geomorphological and Quaternary geological mapping in combination with geochronological studies, has revealed multiple geomorphic, structural and stratigraphic evidence of recent, and probably current, diapiric activity. The activity of the salt system includes general rise in the salt extrusion and subsidence in the flanking withdrawal basins.

The evidence of recent subsidence attributable to salt flow towards the salt wall (salt deflation) is clearer in the Western Basin, including (Fig. 2): (1) Development of large internally drained areas north of the Bolbaite Creek and south of Chella. The former one, around 6 km long, includes a palustrine zone where borehole and geochronological data indicate long-sustained subsidence and aggradation at least since 178 ka (La Roca et al., 1996; Dupré et al., 1998). (2) Defeated and deflected streams. Both subsidence in the salt withdrawal depression, together with uplift in the salt wall, have contributed to block the transverse Bolbaite Creek that used to flow across the salt wall, as record terraces Tt1 and Tt2 and the associated wind gap (Fig. 7). The drainage has been deflected along the withdrawal trough up to Chella, where it flows perpendicularly across the salt wall. (3) Lack of fluvial entrenchment in the Bolbaite and Riajuelo creeks, upstream of major knickpoints at the edge of the salt wall (Chella and Anna).

The salt wall shows multiple evidence of recent activity, with along-strike and transverse variations in the deformation style and strain rates. Evidence of active diapirism in the northwestern and central sector include (Fig. 2): (1) Along-strike differential uplift, as recorded by elevation changes, tilting and warping in strike-parallel remnants of the uppermost tufa terrace. (2) Tilted tufa terraces associated with the margin of the salt extrusion, significantly dipping away from the salt wall. (3) Tufa terraces at the edge of the salt extrusion vertically offset 19-12 m by steep reverse faults dipping into the salt wall (Figs. 5, 6). At the eastern edge of the salt wall, terrace Tt1 shows a well-defined diapiric fault scarp around 18 m high (Fig. 7). This terrace is carved by a wind gap in the upthrown block. Terraces Tt2 and Tt1 and the associated wind gap are related to a paleoBolbaite Creek that used to flow across the salt wall in a more northern position.

In the southeastern sector of the salt wall, where the salt extrusion reaches the largest span, the terraces at the western edge of the salt wall show a different style of deformation (Figs. 8, 10). The detrital terrace Tb2 of the Bolbaite Creek and the tufa terrace Ts4 of the Riajuelo Creek are affected by both synsedimentary subsidence and postsedimentary tilting away from the axis of the salt wall. The deposits of these terraces reach more than 50 m in thickness in a restricted sector at the edge of the salt wall. Moreover, the top of the aggradation surfaces shows an anomalous upstream dip related to differential vertical disp lacement. In this sector, the eastern edge of the salt extrusion does not seem to be a diapiric intrusive contact.

These data indicate along-strike variability of the deformation style along the edges of the salt wall. In the northwestern and central sector, were the salt wall has a more limited width, the salt wall experiences uplift across its full width. However, in the southeastern sector, where the salt wall reaches a larger width, the Quaternary stratigraphic and geomorphic markers indicate general rise, but a restricted fringe affected by subsidence along the western edge of the diapir (Fig. 12). This pattern could be related to: (1) salt mass redistribution within the salt wall, with internal flowage from the edges towards the axis (Chemia, 2008; Warsitzka et al., 2013); (2) insufficient salt flow rate to produce uplift in the full width of the salt wall where it reaches its highest span, probably due to primary salt welds at depth that disconnect the salt wall from the autochthonous salt (Vendeville and Jackson, 1992b); and (3) salt flowage induced by the present-day NW-SE compressional tectonic regime, which may have a higher impact on the SE sector of the salt wall (Roca et al., 2013).

The available geochronological data has significant limitations for the calculation of long-term vertical displacement rates, since eight numerical ages out of ten correspond to minimum age estimates, yielding maximum strain rates. Moreover, most of the dated morpho-stratigraphic markers only allow assessing vertical deformation associated with the diapir edge, rather than the maximum uplift achieved across the full width of the salt wall. Nonetheless, they reveal significant along-strike changes in the rates of vertical displacement consistent with geomorphic and stratigraphic evidence. In the relatively narrow northern and central sector of the salt wall, all the estimated vertical deformation rates, some of them including the full span of the diapir, are consistently ≤0.09 mm/yr. In contrast, in the southern sector, where the diapir is wider and affected by deep entrenchment, long-term rates of differential vertical displacement fall within the range of 0.2-0.4 mm/yr. These values account for the differential vertical displacement associated with the western margin of the diapir, affected by both uplift and marginal subsidence. Higher vertical displacement rates would be obtained computing the cumulative uplift across the full span of the diapir. These values are comparable with those estimated in other active salt structures located in stable continental regions, such us the Paradox Basin, Colorado Plateau, USA (0.5-0.6 mm/yr; Jochems and Pederson, 2015), salt domes of Texas (0.45 mm/yr; Jackson and Seni, 1983), northern Germany (Gorbelen salt dome, 0.1-0.5 mm/yr; Zirngast, 1996) or the Ebro Cenozoic Basin, Spain (~0.3 mm/yr; Lucha et al., 2012). Moreover, as expected, they are much lower than those reported in highly active and prominent diapirs such as Mount Sedom, Israel (5-8 mm/yr; Frumkin, 1996; Weinberger et al., 2006), some salt plugs of the Zagros Mountains (e.g., >4 mm/yr; Bruthans et al., 2010), or Jabal Al Milh diapir, Yemen (4.5 mm/yr; Davison et al., 1996), all in tectonically active regions.

The development of an extruding salt wall along the axis of the graben and the formation of a rising salt ridge has produced significant alterations in the topography and drainage pattern of the Navarrés depression. The salt ridge, locally capped by the uppermost tufa terrace related to a primitive axial drainage, reaches an elevation equivalent to that of the graben margins. The development of the salt ridge represents a striking case of relief inversion, whereby an intrabasinal high has formed by long-sustained diapiric rise where a longitudinal axial drainage and the basin floor once stood. The formation of a strike-parallel intrabasinal water divide and its rise induced a number of alterations in the configuration of the drainage pattern, including (Fig. 2): (1) a change from a longitudinal axial drainage into a dominant longitudinal marginal drainage, controlled by the flanking withdrawal basins; (2) blockage and deflection of transverse drainages that used to flow across the salt wall (e.g. Bolbaite Creek; Fig. 7); (3) development of internally drained subsiding basins; (4) sharp changes in the fluvial style of the transverse drainages separated by abrupt knickpoints, from non-entrenched in the flanking basins to deeply entrenched in the salt extrusion; and (5) variation in the channel pattern within the salt wall and on both sides of the diapir axis, related to gradient attenuation (straight channel) and steepening (sinuous channel with ingrown meanders) (Fig. 11). The stream power excess in the over-steepened section allows the stream to migrate laterally and lengthen the channel, counterbalancing the disequilibrium induced by differential vertical deformation (Harvey, 2007 and references therein).

The Navarrés salt wall shows an area with higher overall relief NE of Chella that resembles a culmination with higher uplift rate (Fig. 11). This sector coincides with the portion of the salt wall that has experienced the deepest fluvial entrenchment (Bolbaite Creek) and the more intense incision. It also includes the sector of the salt wall with higher long-term vertical displacement rates. In the grabens of the Caroch Massif there is a good spatial correlation between the deeply entrenched areas with high differential topographic loading and the distribution of salt walls with prominent relief. All the salt ridges are located in the northern and eastern sectors of the Caroch Massif, close to the regional base level. Moreover, within the Ayora-Cofrentes Graben, the relief created by diapiric activity increases in the areas with deeper fluvial entrenchment and higher erosional unloading. This data suggests that differential loading induced by fluvial entrenchment contributes to enhance diapiric activity in the region. The amount of topographic relief in the grabens of the Caroch Massif region (Table 4) is comparable with those found in other areas where salt flows towards erosionally unloaded valley floors: Canyonlands section of the Colorado Plateau (Jochems and Pederson, 2015; Furuya et al., 2007 and references therein); salt anticlines in the Ebro Cenozoic Basin (Lucha et al., 2008a, b, 2012) and in the Pyrenees, Spain (Gutiérrez et al., 2015); the Ambal salt pillow in the Zagros Mountains (Gutiérrez and Lizaga, 2016); the grabens of Peracalç in the Pyrenees (Gutiérrez et al., 2012) (Table 1). Moreover, Warsitzka et al. (2013) and Peel (2014) illustrate through scaled physical experiments and forward modelling, respectively, that very small amounts of differential loading can initiate salt flowage. The application of DInSAR data could provide deeper insight into the spatial patterns of vertical displacement in these salt systems and their possible relationship with the entrenched drainages (e.g., Aftabi et al., 2010; Barnhart et al., 2012).

7.3. Tectonic activity

Several lines of evidence suggest that the graben-bounding faults lack any evidence of recent surface displacement. The Western Fault is truncated by the youngest Miocene units of the basin fill (Beltrán et al., 1977), and the Eastern Fault is overlapped by non-deformed Pleistocene mantled pediment deposits. Moreover, the faults do not show geomorphic features (e.g., triangular facets, scarps) along their entire length indicative of recent activity. These observations are consistent with the cartographic relationships observed in other grabens. According to Roca et al. (1996), the uppermost Late Miocene conglomerates of the Bicorb basin overlap and truncate the graben-bounding normal faults. The master fault on the western margin of the Ayora-Cofrentes graben is locally onlapped by non-faulted Pliocene sediments (Santisteban et al., 1990; Silva et al., 2015). Nonetheless, we cannot rule out active extensional tectonics in the area. Probably, the development of the salt wall created a weakness zone (strain localizer) that propitiated the migration and concentration of the extensional deformation along the graben axis, as illustrated in experimental models (Vendeville and Jackson, 1992a).

Acknowledgements

The research has been supported by project “SSHAC Level 3 Probabilistic Seismic Hazard Analysis for Spanish Nuclear Power Plant Sites in Spain” (Iberdrola Ingeniería y Construcción) and the Spanish national project CGL2017-85045-P (Ministerio de Economía, Industria y Competitividad). Geochronological analyses were carried out at the Dating Laboratory of the Centro Nacional de Investigación sobre la Evolución Humana (CENIEH).

References

Aftabi, P., Roustaie, M., Alsop, G.I., Talbot, C.J., 2010. InSAR mapping and modelling of an active Iranian salt extrusion. Journal of the Geological Society, London 167, 155-170.

Alberola, A., 1999. Catástrofe, economía y acción política en la Valencia del siglo XVIII. Diputación de Valencia, 333 p.

Alcalá, L., Mazo, A.V., Morales, J., 1985. Mamíferos de las cuencas del Júcar y Cabriel. Museo Nacional de Ciencias Naturales (CSIC), 37 p. http://info.igme.es/cartografiadigital/sidimagenes/magna/20764/Informe%20mam%C3%ADferos/Informe%20mam%C3%ADferos.pdf.

Almalki, K.A., Ailleres, L., Betts, P.G., Bantan, R.A., 2015. Evidence for and relationship between recent distributed extension and halokinesis in the Farasan Islands, southern Red Sea, Saudi Arabia. Arabian Journal of Geosciences 8, 8753-8766.

Anadón, P., Moissenet, E., 1996. Neogene basins in the Eastern Iberian Range. In: P. Friend, P., Dabrio, C.J. (Eds.), Tertiary basins of Spain, the stratigraphic record of crustal kinematics. Cambridge University Press, Cambridge, pp. 68-76.

Anadón, P., Mitjavilla, J.M., Utirlla, R., Vázquez, A., López-Martínez, N., 1995. Radiometric dating and geochemistry of a tuff horizon from a mammal-bearing lacustrine sequence, Miocene Bicorb Basin, Eastern Spain. Revista de la Sociedad Geológica de España 8, 91-98.

Anadón, P., Robles, F., Roca, E., Utrilla, R., Vázquez, A., 1998. Lacustrine sedimentation in the diapir-controlled Miocene Bicorb Basin, Eastern Spain. Paleogeography, Paleoclimatology, Paleoecology 140, 217-243.

Ancochea, E., Huertas, M.J., 2002. Nuevos datos geocronológicos y geoquímicos de las manifestaciones volcánicas de Picasent y Cofrentes (Valencia). Geogaceta 32, 31-34.

Autin, W.J., 2002. Landscape evolution of the Five Islands of south Louisiana: scientific policy and salt dome utilization and management. Geomorphology 47, 227-244

Barnhart, W.D., Lohman, R.B., 2012. Regional trends in active diapirism revealed by mountain range-scale InSAR time series. Geophysical Research Letters 29, L08309.

Bascones, L., Lendínez, A., Martín, D., Tena-Dávila, M., 1979. Mapa Geológico de España a escala 1:50,000 (744, Casas Ibáñez). IGME, 34 p.

Beltrán, F.J., Zapatero, M.A., Rios, L.M., 1977. Mapa Geologico de España 1:50,000 (769, Navarrés). IGME, 28 p.

Bull, W.B., 2007. Tectonic Geomorphology of Mountains. A New Approach to Paleoseismology. Blackwell. Malden, 316 p.

Burbank, D.W., Anderson, R.S., 2012. Tectonic Geomorphology. Wiley-Blackwell. Chichester, 454 p.

Bruthans, J., Filippi, M., Zare, M., Churáčková, Z., Asadi, N., 2010. Evolution of salt diapir and karst morphology during the last glacial cycle: Effects of sea-level oscillation, diapir and regional uplift, and erosion (Persian Gulf, Iran). Geomorphology 121, 291-304.

Carner, J., 2001. Neotectònica de la Vall de Cofrents. Msc. Thesis. Universitat de Barcelona, 49 p.

Castaño, S., Carbó, A., 1995. Los afloramientos triásicos de la zona de confluencia de las Cordilleras Ibérica y Bética. Aportes de la gravimetría a su interpretación. Cuadernos de Geología Ibérica 19, 235-248.

Chemia, Z., 2008. Modeling internal deformation of salt structures targeted for radioactive waste disposal. Acta Universitatis Upsalensis. Digital Comprehensive Summaries of Uppsala Dissertations from the Faculty of Science and Technology 551, 48 p.

Cheng, H., Edwards, R.L., Shen, C.C., Polyak, V.J., Asmeron, Y., Woodhead, J., Hellstrom, J., Wang, Y., Kong, X., Spotl, C., Wang, X., Alexander, E.C., 2013. Improvements in 230 Th and 234U half-life values, and U-Th isotopiuc measurements by multi-collector inductively coupled plasma mass spectrometry. Earth and Planetary Science Letters 371-372, 82-91.

Colman, S.M., 1983. Influence of the Onion Creek salt diapir on the late Cenozoic history of Fisher Valley, southeastern Utah. Geology 11, 240-243.

Davidson, I., Bosence, D., Alsop, G.I., Al-Aawah, H., 1996. Deformation and sedimentation around active Miocene salt diapirs on the Tihama Plain, northwest Yemen. In: Alsop, G.I., Blundell, D.J., Davidson, I. (Eds.), Salt Tectonics. Geological Society, London, Special Publication 100, pp. 23–39.

Dupré, M., Carrión, J., Fumanal, M.P., La Roca, N., Martínez, J., Usera, J., 1998. Evolution and paleoenvironmental conditions of an interfan area in Eastern Spain (Navarés, Valencia). Il Quaternario 11, 95-105.

De Galdeano, C.S., 1990. Geologic evolution of the Betic Cordilleras in the Western Mediterranean, Miocene to present. Tectonophysics 172, 107-119.

De Ruig, M.J., 1995. Extensional diapirism in the Eastern Prebetic Foldbelt, Southeastern Spain. In: Jackson, M.P.A., Roberts, D.G., Snelson, S. (Eds.), Salt tectonics: a global perspective. AAPG Memoir 65, pp. 353-367.

Erol, A.O., 1989. Engineering geological considerations in a salt dome region surrounded by sabkha sediments, Saudi Arabia. Engineering Geology 26, 215-232.

Escosa, F. O., Roca, E., Ferrer, O., 2018a. Testing thin-skinned inversion of a prerift salt-bearing passive margin (Eastern Prebetic Zone, SE Iberia). Journal of Structural Geology 109, 55–73.

Escosa, F.O., Ferrer, O., Roca, E., 2018b. Geology of the Eastern Prebetic Zone at the Jumilla region (SE Iberia). Journal of Maps 14, 77-86.

Frumkin, A., 1996. Uplift rate relative to base-levels of a salt diapir (Dead Sea Basin, Israel) as indicated by cave levels. In: Alsop, G.I., Blundell, D.J., Davison, I. (Eds.), Salt tectonics. Geological Society London Special Publication 100, pp. 41-47.

Furuya, M., Mueller, K., Wahr, J., 2007. Active salt tectonics in the Needles District, Canyolands (Utah) as detected by Interferometric Synthetic Aperture Radar and Point Target Analysis. Journal of Geophysical Research 112, B06418.

Galbraith, R.F., Roberts, R.G., 2012. Statistical aspects of equivalent dose and error calculation and display in OSL dating: an overview and some recommendations. Quaternary Geochronology 11, 1-27.

Gaullier, V.; Vendeville, B.C., 2005. Salt tectonics driven by sediment progradation: Part II-Radial spreading of sedimentary lobes prograding above salt. AAPG Bulletin 89, 1081-1089.

García, A., García, L., 1979. Mapa Geológico de España a escala 1:50,000 (746, Llombay). IGME, 39 p.

Ge, H.X., Jackson, M.P.A., Vendeville, B.C., 1997. Kinematics and dynamics of salt tectonics driven by progradation. AAPG Bulletin 81, 398-423.

Giner-Robles, J.L., Silva, P.G., Rodríguez-Pascua, M.A., Pérez-López, R., Alberola-Romá, A., 2014. Efectos geológicos y arqueológicos producidos por el terremoto de Estubeny de 1748 AD (SE de España). Resúmenes de la 2ª Reunión Ibérica sobre Fallas Activas y Paleosismología. Lorca, Spain, pp. 149-152.

Gutiérrez, F., Gutiérrez, M., 2016. Landforms of the Earth. An illustrated guide. Springer, 270 p.

Gutiérrez, F., Ortí, F., Gutiérrez-Elorza, M., Pérez-González, A., Benito, G., Gracia-Prieto, J., Durán, J.J., 2001. The stratigraphical record and activity of evaporite dissolution subsidence in Spain, Carbonates and Evaporites 16, 46-70.

Gutiérrez, F., Gutiérrez, M., Gracia, F.J., McCalpin, J.P., Lucha, P., Guerrero, J., 2008. Plio-Quaternary extensional seismotectonics and drainage network development in the central sector of the Iberian Range (NE Spain). Geomorphology 102, 1, 21-42.

Gutiérrez, F., Linares, R., Roqué, C., Zarroca, M., Rosell, J., Galve, J.P., Carbonell, D., 2012b. Investigating gravitational grabens related to lateral spreading and evaporite dissolution subsidence by means of detailed zapping, trenching, and electrical resistivity tomography (Spanish Pyrenees). Lithosphere 4, 331-353.

Gutiérrez, F., Carbonel, D., Kirkham, R.M., Guerrero, J., Lucha, P., Matthews, V., 2014. Can flexural-slip faults related to evaporite dissolution generate hazardous earthquakes? The case of the Grand Hogback Monocline of west-central Colorado. GSA Bulletin 126, 1481-1494.

Gutiérrez, F., Linares, R., Roqué, C., Zarroca, M., Carbonel, D., Rosell, J., Gutiérrez, M., 2015. Large landslides associated with a diapirc fold in Canelles Reservoir (Spanish Pyrenees). Detailed geological-geomorphological mapping, trenching and electrical resistivity tomography. Geomorphology 241, 224-242.

Gutiérrez, F., Lizaga, I., 2016. Sinkholes, collapse structures and large landslides in an active salt dome submerged by a reservoir. The unique case of the Ambal ridge in the Karun River, Zagros Mountains, Iran. Geomorphology, 254, 88-103Harrison, T.S. (1927). Colorado-Utah salt domes. AAPG Bulletin 11, 111-133.

Harvey, A., 2007. High-sinuosity bedrock channels: response to rapid incision. Examples in NE Spain. Cuaternario y Geomorfología 21, 21-47.

Holford, S., Thomson, K., Gaffney, V., 2007. Salt tectonics in the Southern North Sea: controls on late Pleistocene-Holocene geomorphology. In: Gaffney, V., Thomson. K., Fitch, S. (Eds.), Mapping Doggerland. The Mesolithic Landscapes of the Southern North Sea. Archaeopres, Oxford, pp. 61-5.

Hudec, M.R., Jackson, M.P.A., 2007. Terra infirma: understanding salt tectonics. Earth-Science Reviews 82, 1-28.

Hudec, M.R., Jackson, M.P.A., 2011. The salt mine: a digital atlas of salt tectonics: Austin, TX, The University of Texas at Austin, Bureau of Economic Geology, Udden Book Series 5; Tulsa, OK, American Association of Petroleum Geologists, Memoir 99, 305 p.

Huntoon, P.W., 1982. The Meander anticline, Canyonlands, Utah: An unloading structure resulting from horizontal gliding on salt. Geological Society of America Bulletin 93, 941-950.

IGME, 1989. Las aguas subterráneas en la Comunidad Valenciana. Uso, calidad y perspectivas de utilización. IGME, Madrid, 289 p.

Ivanovich, M., Harmon, R.S., 1992. Uranium-series disequilibrium: applications to earth, marine, and environmental sciences. 2nd edition, Clarendon Press.

Jackson, M.P.A., Seni, S.J., 1983. Geometry and evolution of salt structures in a marginal rift basin of the Gulf of Mexico, East Texas. Geology 11, 131-135.

Jackson, M.P.A., Talbot, C.J., 1986. External shapes, strain rates, and dynamics of salt structures. Geological Society of America Bulletin 97, 305-323.

Jahani, S., Callot, J.P., Frizon de Lamotte, D., Letouzey, J., Leturmy, P., 2007. The salt diapirs of the eastern Fars Province (Zagros, Iran): A brief outline of their past and present. In: Lacombe, O., Roure, F., Lavé, J., Vergés, J. (Eds.), Thrust Belts and Foreland Basins. Springer, pp. 289-308.

Jochems, A.P.; Pederson, J.L., 2015. Active salt deformation and rapid, transient incision along the Colorado River near Moab, Utah. Journal of Geophysical Research: Earth Surface 120, 730-744.

Keller, E.A., Pinter, N., 1996. Active Tectonics. Earthquakes, Uplift and Landscape. Prentice Hall. New Jersey, 338 p.

Kirkham, R.M., and Scott, R.B., 2002, Introduction to late Cenozoic evaporite tectonism and volcanim in west-central Colorado. In: Kirkham, R.M., Scott, R.B., and Judkins, T.W. (Eds.), Late Cenozoic evaporite tectonism and volcanism in west-central Colorado: Geological Society of America Special Paper 366, pp. 1-14.

Köthe, A., Hoffman, N., Krull, P., Zirngast, M., Zwirner, R., 2007. Geology of the overburden and adjoining rock of the Gorleben salt dome. Bundesanstalt für Geowisserschaften und Rohstofee, 220 p.

Kravitz, K., Upton, P., Roy, S.G., 2017. Topographic controlled forcing of salt flow: Three-dimensional models of an active salt system, Canyonlands, Utah. Journal of Geophysical Research: Solid Earth 122, 710-733.

La Roca, N., Fumanal, M.P., Martínez, J., 1996. Evolución cuaternaria del drenaje en un corredor intramontano: La Canal de Navarés (Valencia, Spain). In: Grandal d'Anglade, A., Pagés, J. (Eds.), Cadernos Laboratorio Xeológico de Laxe 21, 445-455.

Lang, J., Hampel, A., Brandes, C., Winsemann, J., 2014. Response of salt structures to ice-sheet loading: implications for ice-marginal and subglacial processes. Quaternary Science Reviews 101, 217-233.

Lee, G.H., Watkins, J.S., Bryant, W.R., 1996. Bryant Canyon Fan System: an unconfined, large river-sourced system in the Northwestern Gulf of Mexico. AAPG Bulletin 80, 340-358.

Lendínez, A., Tena, M., 1976a. Mapa Geológico de España a escala 1:50,000 (745, Jalance). IGME, 28 p.

Lendínez, A., Tena, M., 1976b. Mapa Geológico de España a escala 1:50,000 (767, Carcelén). IGME, 28 p.

Lendínez, A., Tena, M., 1978. Mapa Geológico de España a escala 1:50,000 (793, Almansa). IGME, 31 p.

López, G.I., Goodman-Tchernov, B.N., Porat, N., 2018. OSL over-dispersion: A pilot study for the characterization of extreme events in the shallow marine realm. Sedimentary Geology 378, 35-51.

Lucha, P., Cardona, P., Gutiérrez, F., Guerrero, J., 2008a. Natural and human-induced dissolution and subsidence processes in the salt outcrop of the Cardona Diapir (NE Spain). Environmental Geology 53, 1023-1035.

Lucha, P., Gutiérrez, F., Guerrero, J., 2008b. Anomalías geomorfológicas y deformaciones cuaternarias en el sistema fluvial del Cardener y su relación con el crecimiento de anticlinales salinos y fenómenos de subsidencia por disolución de evaporitas. In: Benavente, J., Gracia, F.J. (Eds.), Trabajos de Geomorfología en España 2006-2008. SEG. Cádiz, pp. 53-56.

Lucha, P., Gutiérrez, F., Galve, J.P., Guerrero, J., 2012. Geomorphic and stratigraphic evidence of incision-induced halokinetic uplift and dissolution subsidence in transverse drainages crossing the evaporite-cored Barbastro-Balaguer Anticline (Ebro Basin, NE Spain). Geomorphology 171-172, 154-172.

Martí, J., Mitjavila, J., Aparicio, A., 1992. Cenozoic magmatism of the Valencia trough (western Mediterranean): relationship between structural evolution and volcanism. Tectonophysics 203, 145-165.

Martin, R.G., Bouma, A.H., 1981. Active diapirism and slope steepening, Northern Gulf of Mexico Continental Slope. Marine Geotechnology 5, 63-91.

Martínez del Olmo, W., Motis, K., Martín, D., 2015. El papel del diapirismo de la sal triásica en la estructuración del Prebético (SE de España). Revista de la Sociedad Geológica de España 28, 3-24.

Martínez-Solares, J.M., Mezcua, J., 2002. Catálogo sísmico de la Península Ibérica 8880 a.C.-1900). Ministerio de Fomento, 253 p.

Mazo, A.V., 1997. El yacimiento rusciniense de Alcalá de Júcar (Albacete). Taxonomía y bioestratigrafía. Estudios Geológicos 53, 275-286.

Michetti, A.M., Esposito, L., Guerrieri, L., Porfido, S., Serva, L., Tatevossioan, R., Vittori, E., Audemard, F., Azuma, T., Clague, J., Comerci, V., Gurpinar, A., McCalpin, J., Mohammadioun, B., Morner, N.A., Ota, Y., Roghozin, E., 2007. Intensity Scale ESI 2007. In: Guerrieri, L., Vittori, E. (Eds.), Memoria Descrittive Carta Geologia d?Italia, 74, Servizio Geologico d'Italia-Dipartimento Difesa del Suolo, APAT, Roma, 53 p.

Moissenet, E., 1985. Les dépressions tarditectoniques des Chaînes Ibériques méridionales: distension, diapirisme et dépôts néogènes associés. C.R. Acad. Sc. Paris 300, 523-528.

Olivera, C., Susagna, T., Roca, A., Goula, X., 1992. Seismicity of the Valencia trough and surrounding areas. Tectonophysics 203, 99-109.

Ortí, F., 1974. El Keuper del Levante español. Estudios Geológicos 30, 7-46.

Ortí, F., 1990. Keuper de Cofrentes. In: Ortí, F., Salvany, J.M. (Eds.). Formaciones evaporíticas de la Cuenca del Ebro y cadenas periféricas, y de la zona de levante. ENRESA-Universidad de Barcelona, pp. 283-287.

Ortí, F., 2004. Últimas etapas de actividad del rifting. Sedimentos asociados. In: Vera, J.A. (Ed.), Geología de España. IGME-SGE, pp. 492-495.

Pedley, H.M., 1990. Classification and environmental models of cool freshwater tufas. Sedimentary Geology 68, 143-154.

Peel, F.J., 2014. How do withdrawal minibasins form? Insights from forward modelling, and implications for hydrocarbon migration. Tectonophysics 630, 222-235.

Pérez, N.M., Nakai, S., Wakita, H., Albert-Bertrán, J.F., Redondo, R., 1996. Preliminary results on $^{3}He/^{4}He$ isotopic ratios in terrestrial fluids from the Iberian península: seismotectonic and neotectonic implications. Geogaceta 20, 830-833.

Popenoe, P., Schmuck, E.A., Dillon, W.P., 1993. The Cape Fear landslide: Slope failure associated with salt diapirism and gad hydrate decomposition. In: Schwab, W.C., Lee, H.J., Twichell, D.C. (Eds.), Submarine landslides: Selected studies in the U.S. Exclusive Economic Zone. U.S. Geological Survey Bulletin 2002, pp. 40-53.

Prescott, J.R., Hutton, J.T., 1994. Cosmic ray contributions to dose rates for luminescence and ESR dating: large depths and long-term time variations. Radiation Measurements 23, 497-500.

Quintero, I., Almela, A., Gómez, E., Mansilla, H., 1978. Mapa Geológico de España a escala 1:50,000 (792, Alpera). IGME, 47 p.

Refice, A., Pasquariello, G., Bovenga, F., Festa, V., Acquafredda, P., Spilotro, G., 2016. Investigating uplift in Lesina Marina (Southern Italy) with the aid of persistent scatterer SAR interferometry and in situ measurements. Environmental Earth Sciences 75, 243.

Roca, E., Guimerà, J., 1992. The Neogene structure of the eastern Iberian margin: structural constraints on the crustal evolution of the Valencia trough (western Mediterranenan). Tectonophysics 203, 203-218.

Roca, E., Anadón, P., Utrilla, R., Vázquez, A., 1996. Rise, closure and reactivation of the Bicorb-Quesa evaporite diapir, Eastern Prebetics, Spain. Journal of the Geological Society, London 153, 311-321.

Roca, E., Sans, M., Koyi, H.A., 2006. Polyphase deformation of diapiric areas in models and in the eastern Prebetics (Spain). AAPG Bulletin 90, 115-136.

Roca, E., Beamud, E., Rubinat, M., Soto, R., Ferrer, O., 2013. Paleomagnetic and inner diapiric structural constraints on the kinematic evolution of a salt-wall: The Bicorb-Quesa and northen Navarrés salt-wall segments case (Prebetic Zone, SE Iberia). Journal of Structural Geology 52, 80-95.

Rodríguez-Estrella, T., 1983. Neotectónica relacionada con las estructuras diapíricas en el Sureste de la Península Ibérica. Tecniterrae 51, 14-30.

Rodríguez-Estrella, T., Pulido-Bosch, A., 2010. Gypsum karst evolution in a diapir: a case study (Pinoso, Alicante, Spain). Environmental Earth Sciences 59, 1057-1063.

Rubinat, M., Ledo, J., Roca, E., Rosell, O., Queralt, P., 2010. Magnetotelluric characterization of a salt diapir: a case study on Bicrob-Quesa Diapir (Prebatic Zone, SE Spain). Journal of the Geological Society, London 167, 145-153.

Rubinat, M., Roca, E., Escalas, M., Queralt, P., Ferrer, O., Ledo, J.J., 2013. The influence of basement structure on the evolution of the Bicorb-Quesa Diapir (Eastern Betics, Iberian Peninsula): contractive thin-skinned deformation above a pre-existing extensional basement fault. International Journal of Earth Sciences 102, 25-41.

Ruiz, V., 1976. Mapa Geológico de España a escala 1:50,000 (768, Ayora). IGME, 34 p.

Sáenz-Ridruejo, C., López-Mariñas, J.M., 1975. La edad del volcanismo de Cofrentes (Valencia) Tecniterrae 6, 8-14.

Santisteban, C., Ruiz-Sánchez, F.J., Bello, D., 1989. Los depósitos lacustres del Terciario de Bicorb. Acta Geologica Hispánica 24, 299-307.

Santisteban, C., Ruiz-Sánchez, F.J., Lacomba, J.I., 1993. Ambiente sedimentario y edad de la unidad superior de brechas de la cuenca de Quesa (Provincia de Valencia). Estudios Geológicos 49, 337-342.

Santisteban, C., Saiz, J., Bello, D., Ruiz-Sánchez, F.J., 1990. Tectónica y sedimentación en el margen oeste del rift terciario del valle de Ayora-Cofrentes (Valencia). Geogaceta 8, 44-47.

Santisteban, C., Ruiz-Sánchez, F.J., Lacomba, J.I., 1994. Estratigrafía, edad y evolución de los depósitos terciarios de la cuenca de antepaís de Quesa-Bicorb (Valencia). Comunicaciones al II Congreso del Grupo Español del Terciario, Jaca, pp. 209-212.

Seghedi, I., Brändle, J.L., Szakács, A., Ancochea, E., Vaselli, O., 2002. El manto litosférico en el sureste de España: Aportaciones de los xenolitos englobados en rocas alcalinas del mio-plioceno. Geogaceta 32, 27-30.

Silva, P.G., Rodríguez-Pascua, M.A., Giner-Robles, J., Pérez-López, R., Lario-Gómez, J., Perucha-Atienza, M.A., Bardají-Azcárate, T., Huerta-Hurtado, P., Roquero, E., Bautista, M.B., 2014. Catálogo de los efectos geológicos de los terremotos de España. IGME-AEQUA, 358 p.

Silva, P.G., Giner-Robles, J.L., Elez, J., Rodríguez-Pascua, M.A., Perucha, M.A., Roquero, E., Huerta, P., Martínez-Graña, A., 2015. Tectonic geomorphology and volcanism in the Ayora-Cofrentes tectonic corridor, Valencia (Prebetic, SE Spain). XIV Reunión Nacional de Cuaternario, Granada, pp. 162-166.

Simón, J.L., 1989. Late Cenozoic stress field and fracturing in the Iberian Chain and Ebro Basin (Spain). Journal of Structural Geology 11, 285-294.

Sirocko, F., Szeder, T., Seelos, C., Lehne, R., Rein, B., Schneider, W.M., Dimke, M., 2002. Young tectonic and halokinetic movements in the North-German-Basin: its effect on formation of modern rivers and surface morphology. Netherlands Journal of Geosciences 81, 431-441.

Sopeña, A., Ramos, A., Villar, M.V., 1990. El Triásico del sector Alpera-Montealegre del Castillo (Prov. de Albacete). In: Ortí, F., Salvany, J.M. (Eds.), Formaciones evaporíticas de la Cuenca del Ebro y cadenas periféricas, y de la zona de levante. ENRESA-Universidad de Barcelona, pp. 224-231.

Soubrier, J., García, L., Muelas, A., García, A., 1976. Mapa Geológico de España a escala 1:50,000 (721, Cheste). IGME, 39 p.

Stich, D., Martín, R., Batlló, J., Macià, R., Mancilla, F., Morales, J., 2018. Normal faulting in the 1923 Berdún earthquake and postorogenic extension in the Pyrenees. Geophysical Research Letters 45, 3026–3034.

Suárez-Alba, J., 2007. La Mancha Triassic and Lower Lias stratigraphy, a well log interpretation. Journal of Iberian Geology 33, 55-78.

Talbot, C.J., Alavi, M., 1996. The past of a future syntaxis across the Zagros. Geological Society London Special Publication 100, 89-109.

Tripsanas, E.K., Bryant, W.B., Phaneuf, B.A., 2004. Slope-instability processes caused by salt movements in a complex deep-water environment, Bryant Canyon area, northwest Gulf of Mexico. AAPG Bulletin 88, 801-823.

Trudgill, B., 2002. Structural controls on drainage development in the Canyonlands grabens of southeast Utah. AAPG Bulletin 86, 1095-1112.

Vendeville, B.C., Jackson, M.P.A., 1992a. The rise of diapirs during thin-skinned extension. Marine and Petroleum Geology 9, 331-353.

Vendeville, B.C., Jackson, M.P.A., 1992b. The fall of diapirs during thin-skinned extension. Marine and Petroleum Geology 9, 354-371.

Vera, J.A., Martín-Algarra, A., 2004. Cordillera Bétrica y Baleares. Divisiones mayores y nomenclatura. In: Vera, J.A. (Ed.), Geología de España. IGME-SGE, pp. 348-350.

Warren, J.K., 2016. Evaporites. A Geological compendium. Springer, 1813 p.

Warsitzka, M., Kley, J., Kukowski, N., 2013. Salt diapirism driven by differential loading. Some insights from analogue modelling. Tectonophysics 591, 83-97.

Weinberger, R., Lyakhovsky, V., Baer, G., Begin, Z.B., 2006. Mechanical modelling and InSAR measurements of Mount Sedom uplift, Dead Sea basin: Implications for effective viscosity of rock salt. Geochemistry, Geophysics, Geosystems 7, Q05014.

Zarei, M., Raeisi, E., Talbot, C., 2012. Karst development on a mobile substrate: Konarsiah salt extrusion, Iran. Geological Magazine 149, 412-422.

Zirngast, M., 1996. The development of the Gorbelen salt dome (NW Germany) based on quantitative analysis of peripheral sinks. In: Alsop, G.I., Blundell, D.J., Davidson, I. (Eds.), Salt Tectonics. Geological Society, London, Special Publication 100, pp 203–226.

Figure captions

Figure 1. Morpho-structural sketch on shaded relief model of the Caroch Massif region depicting the distribution of post-orogenic grabens, Neogene graben-fill sediments, outcrops of Triassic evaporites (Keuper facies), the main drainage network (entrenched and non-entrenched), knick points and poorly- or internally-drained areas. Geological data derived from the Spanish geological sheets at 1:50,000 scale (Ruiz, 1976; Lendínez and Tena, 1976a, 1976b, 1978; Subrier et al., 1976; Beltrán et al., 1977; Bascones et al., 1979; García and García, 1979).

Figure 2. Geological-geomorphological map of the Navarrés graben and salt wall.

Figure 3. Generalised cross-section across the Navarrés graben and salt wall.

Figure 4. Eastern Fault of Navarrés graben juxtaposing upturn Cretaceous strata against Miocene conglomerates and truncated by non-deformed old mantled-pediment deposit. Outcrop located at coordinates 30S 0698560 7 4334008.

Figure 5. Tufa terraces north of Navarrés village affected by diapiric deformation at the SW edge of the salt wall. A: Photograph showing tufa terraces Tw1 and Tw2 offset by a steep reverse fault. B: Sketch integrating the geometrical relationships observed in the field and the relative position of the samples collected for U/Th dating. Terrace Tw1 occurs on both sides of the reverse fault, whereas terrace Tw2 is restricted to the downthrown side. The samples with no age were discarded due to evidence of alteration and precipitation of secondary carbonate. C: Reverse fault juxtaposing Triassic sediments against tufa terrace Tw2.

Figure 6. Reverse fault at the western edge of the salt wall (Navarrés village), juxtaposing Triassic sediments against tufa deposits ascribed to terrace Tw2.

Figure 7. Annotated shaded relief model showing tufa terraces Tt1 and Tt2, faulted at the eastern edge of the salt wall and a wind gap carved into terrace Tt1. Red arrows indicate

inclination of geomorphic surfaces. The stars indicate position of OSL- and U/Th-dated samples.

Figure 8. Detrital terrace of the Bolbaite Creek (Tb2), downstream of the Chella water fall, thickened at the edge of the salt wall and tilted away from the diapir axis. Photograph taken from 30S 702438 7 4324503. The stars indicate the position of OSL-dated samples.

Figure 9. The tortuous Bolbaite Creek in the downstream flank of the salt wall, where differential diapiric uplift contributes to increase the channel gradient and the stream power, stimulating lateral migration and the development of ingrown bedrock meanders. Tilted terrace Tb3 in the background. Photograph taken from 30S 703600 7 4324607.

Figure 10. Tufa (terrace Ts4) and alluvial deposits in Anna quarry, thickened at the edge of the salt wall and tilted away (upstream) form the diaper axis. Star indicate location of dates tufa sample. Photograph taken from 30S 704418 / 4321172.

Figure 11. Shaded relief model showing an oval shaped culmination of the salt wall with higher relief, flanked by the Eastern and Western basins. This area coincides with the most deeply entrenched and more intensely dissected sector of the salt wall. Note the increase in the sinuosity of the Bolbaite Creek downstream of the topographic axis of the diapir. S.I: stands for sinuosity index (length of channel in a section/length of section). Red arrows indicate tilted terraces.

Figure 12. Diagram showing along-strike variability in the deformation styles. See explanation in the text.

Table 1

Geological setting	Salt structure	Salt flow	Geomorphic and stratigraphic evidence	Local relief (m)	Rates of surface displacement	References
Laramide folds, Colorado Plateau, Utah	Onion Creek salt wall (Carboniferous Paradox Basin)	Differential flow induced or enhanced by incision-induced unloading	Subsidence basin filled by 125 m of Plio-Pleistocene deposits and blockage and diversion of Fisher Creek	500	-	Colman (1983)
Laramide folds, Colorado Plateau, Utah	Salt-Cache salt wall (Carboniferous Paradox Basin)	Differential vertical deformation related to salt flow induced by incision-induced unloading	Thickened terraces affected by subsidence and upwarped strath terraces	500	-0.5-0.6 mm/yr	Jochems and Pederson (2015)
Colorado Plateau, Paradox Basin, Utah	Sinuous salt anticline (Meander Anticline) controlled by the deeply entrenched Cataract Canyon	Down-dip flow driven by differential unloading due to incision of the Colorado River	Dome-shaped culminations with topographic expression	450	+2-3 mm/yr (DInSAR, LOS)	Harrison (1927); Huntoon (1982); Furuya et al. (2007)
Carbondale Collapse Center associated with the Pennsylvanian Eagle Valley Evaporite Formation, Southern Rocky Mountains, Colorado	Local salt anticlines controlled by the entrenched drainage network	Salt flow towards the erosionally unloaded valleys	Valley-centered anticlines and uparched Quaternary fluvial terraces dipping away from valley axis. Differential uplift in a single terrace as high as 30 m	700	-	Kirkham et al. (2002); Gutiérrez et al. (2014)
Gulf of Mexico continental slope, Texas-Louisiana	Local diapiric uplift (Jurassic Louann Salt) in the bottom of the Alaminos Canyon	Salt flow towards the erosionally unloaded bottom of the canyon, resulting in its blockage and the creation of an elongated enclosed basin (Gyre Basin)	Topographic high in the bottom of the blocked canyon. Uplifted deposits previously deposited in the canyon floor	550-750	+20 mm/yr (biostratigraphically dated deposits)	Martin and Bouma (1981)
Gulf of Mexico continental slope, Texas-Louisiana	Bryant Canyon, generated by the ancestral Mississippi River. Path controlled by salt-withdrawal minibasins	Salt flow towards the erosionally unloaded canyon, eventually leading to its obliteration	Deformed Quaternary deposits, oversteepened slopes and slumps, local blocking of canyon, partial obliteration of the erosional depression by differential diapirc uplift	300-800		Lee et al. (1996); Tripsanas et al. (2004)
Salt-bearing Miocene Gachsaran Fm. in the Dezful Embayment, Zagros Mountain, Iran	Salt pillow (Ambal ridge) associated with the deeply entrenched Karun River	Salt flow controlled by transverse fault and favoured by the erosionally unloaded Karun River valley	Forms a ridge 245 m in local relief associated with a major river. The river channel is deflected around the salt ridge. Tributary drainages blocked at the edge of the salt structure	500	-	Gutiérrez and Lizaga (2016)
Ebro Cenozoic Basin, foreland basin of the Pyrenees, NE Spain	Cardona salt stock	Salt extrusion developed where the Cardener River has beached a salt anticline	Hill 150 m high of exposed salt. Pliocene or Quaternary deposits with dome structure concordant with the topography and rim depression	200	ca +1mm/yr (geodetic)	Wagner et al. (1971), Lucha et al. (2008a)
Ebro Cenozoic Basin, foreland basin of the Pyrenees, NE Spain	Salt anticlines traversed by the Cardener River	Salt flowage probably enhanced by the entrenchment of the transverse Cardener River	Terraces upwarped and tilted upstream. Channel sinuosity variations related to gradient changes caused by the growing anticlines	200-400	-	Lucha et al. (2008b)
Ebro Cenozoic Basin, foreland basin of the Pyrenees, NE Spain	Salt anticline traversed by the Cinca and Noguera-Ribagorzana rivers	Strike-parallel salt flow towards the valley floor due to differential loading caused by fluvial entrenchment	Terraces tilted away from the valley	100-150	>+0.3 mm/yr (OSL-dated tilted terrace)	Lucha et al. (2012)

South Pyrenean Zone, Pyrenees, NE Spain	Tectonically-thickened Triassic evaporites associated with a thrust and overlain by brittle carbonate rocks	Lateral flow of the Triassic evaporites towards a debuttressed and unloaded erosional escarpment ca 450 m high	Bulging in the lower part of the escarpment. Horst and graben morphostructure in the brittle caprock. Fault scarps with anomalous aspect ratios. Disrupted drainage expressed by wind gaps, hanging valleys and defeated streams	450	-	Gutiérrez et al. (2012)
South Pyrenean Zone, Pyrenees, NE Spain	Salt anticline traversed by the Noguera-Ribagorzana river with local extrusion associated with deeply entrenched valley floor	Strike-parallel salt flow towards the erosionaly unloaded valley floor	Dome-shaped extrusion and deflected tributary drainages. Crestal graben in anticline at valley margin. Recent terrace tilted upstream and overthrusted by diapiric rocks	500	-	Gutiérrez et al. (2015)

Table 1. Examples of erosion-induced salt flowage. The reported geomorphic and stratigraphic evidence of active salt flow is indicated, together with rates of surface displacement (positive and negative values indicate uplift and subsidence, respectively). DiNSAR: Differential Interferometic Synthetic Aperture Radar. LOS: Line-of-sight.

Table 2

Sample code[a]	Lab code[b]	Burial depth (m)[c]	Water content (%)[d]	Aliquots[e]	$\dot{D}_{Beta}$ (Gy/ka)	$\dot{D}_{Gamma}$ (Gy/ka)	$\dot{D}_{Cosmic}$ (Gy/ka)	^{238}U (ppm)	^{232}Th (ppm)	^{40}K (%)	Total $\dot{D}$ (Gy/ka)	D_E (Gy)	Age (ka)[f]	OD (%)[g]/Age model
C-WG-OSL1	LM-17113-01	3.9	14.92±0.28	18/24	1.60±0.04	0.903±0.032	0.132±0.02	2.95±0.03	12.64±0.30	1.68±0.05	2.097±0.047	368±20	176±10	48.3/MAM
C-CHE-OSL3	LM-17113-03	44	27.73±0.59	24/24	0.30±0.02	0.214 ±0.008	0.0±0.0	1.32±0.04	2.81±0.08	0.33±0.01	0.360±0.015	59±2	164±9	15/CAM
C-CHE-OSL4	LM-17113-03	25	24.03±0.45	24/24	0.30±0.02	0.198±0.007	0.025±0.02	1.00±0.01	2.17±0.01	0.23±0.03	0.385±0.025	53±1.4	138±10	13/CAM

[a] Original sample code

[b] Code assigned by the Laboratory

[c] Depth below top aggradation surface measured at sampling site

[d] Assumed to be 60% of the maximum saturation value measured in the laboratory

[e] Number of aliquots used for De calculation versus total aliquots measured

[f] Reference year for ages is 2018. Reported errors are at 1σ and incorporate systematic uncertainties of dose and water content, as well as errors associated with the determination of D_E

[g] Overdispersion reflects precision beyond instrumental errors; values of ≤20% indicate low dispersion in equivalent dose values and unimodal distribution. MAM: minimum age model; CAM: central age model

Table 2. Optically Stimulated Luminescence (OSL) ages on quartz grains from samples collected in Quaternary fluvial deposits. The size range of quartz grains used for the OSL measurements was 90-125 µm for all the samples.

Table 3

Sample code	Lab code	Facies	U [µg g^{-1}]	Th [µg g^{-1}]	$^{230}Th/^{232}Th \times 10^{-6}$ [at/at]	$\delta^{234}U$[meas]	$\delta^{234}U_{init}$ [calc]	$^{230}Th/^{238}U$[act/act]	^{230}Th [yr]	^{230}Th corr [yr]
C-NA-SU1	SU-17113-07	Stromatolitic lamination	0.236 (0.002)	0.0828 (0.003)	53 (1)	130 (2)	257 (20)	1,132 (0.006)	359,500 (20,000)	241,020 (15,000)
C-NA-SU4	SU-17113-10	Phytoclasts	0.185 (0.003)	0.150 (0.003)	22 (1)	169 (3)	251 (20)	1,088 (0.003)	245,134 (12,257)	140,676 (7,050)
C-NA-SU5	SU-17113-11	Phytoherm	0.220 (0.003)	0.045 (0.003)	86 (1)	148 (3)	268 (21)	1,069 (0.003)	249,629 (12,481)	211,039 (10,552)
C-WG-SU3	SU-17113-03	Stromatolitic lamination	0.285 (0.003)	0.233 (0.003)	27 (1)	435 (3)	668 (21)	1,353 (0.004)	225,459 (11,273)	149,722 (7,487)
C-WG-SU1	SU-17113-01	Laminated oncoid	0.242 (0.002)	0.155 (0.008)	34 (1)	336 (2)	199 (22)	1,328 (0.004)	280,595 (13,245)	186,404 (6,254)
C-WG-SU2	SU-17113-02	Oncoid	0.238 (0.002)	0.067 (0.003)	86 (1)	407 (1)	189 (21)	1,477 (0.006)	341,009 (7,059)	272,310 (4,220)
C-AN-SU1	SU-17113-04	Phytoclasts	0.118 (0.003)	0.0690 (0.003)	26 (1)	456 (3)	573 (20)	0.936 (0.003)	105,312 (5,270)	79,304 (3,965)

Table 3. Measurements and age estimates obtained from the analysed tufa samples. Values in parenthesis indicate the 2σuncertianty. Decay constants used in the calculations: λ_{238}= 1.55125x10^{-10}; λ_{234}= 2.82206x10^{-6}; λ_{230}= 9.1705x10^{-6}.

Table 4

Basin	**Trend**	**Length/Width (km)**	**Salt wall**	**Neogene fill**	**Dissection**	**Local relief of graben depression (m)**	**Relief of diapiric rocks (m)**
Júcar	E-W	26/5	no	Mio-Pliocene	yes	450	-
Carcelén	E-W	32/5	no	Mio-Pliocene	no	370	-
Las Rochas	ENE-WSW, E-W	16/3	no	Mio-Pliocene	no	150	-
Alpera	N-S	46/13	no	Mio-Pliocene	no	240	-
Ayora-Cofrentes	N-S	46/6	yes (N), no (S)	Mio-Pliocene	yes (N), no (S)	450 (N), 320 (S)	150
Cortés de Pallés	ENE-WSW	15/3	yes	Mio-Pliocene	yes	550	300
Sácaras	NNW-SSE,NW-SE	20/3.5	no	no	no	440	-
Bicorb-Quesa	ENE-WSW	24/5	yes	Middle-Late Miocene	yes	300	350
Navarrés	NNW-SSE	20/4.5	yes	Miocene	yes	300	150
Tous	NNW-SSE	19/2	no	no	yes	200	-

Table 4. Structural, stratigraphic and topographic features of the different grabens in the Caroch Massif region.

Figure (Color) 1
Click here to download high resolution image

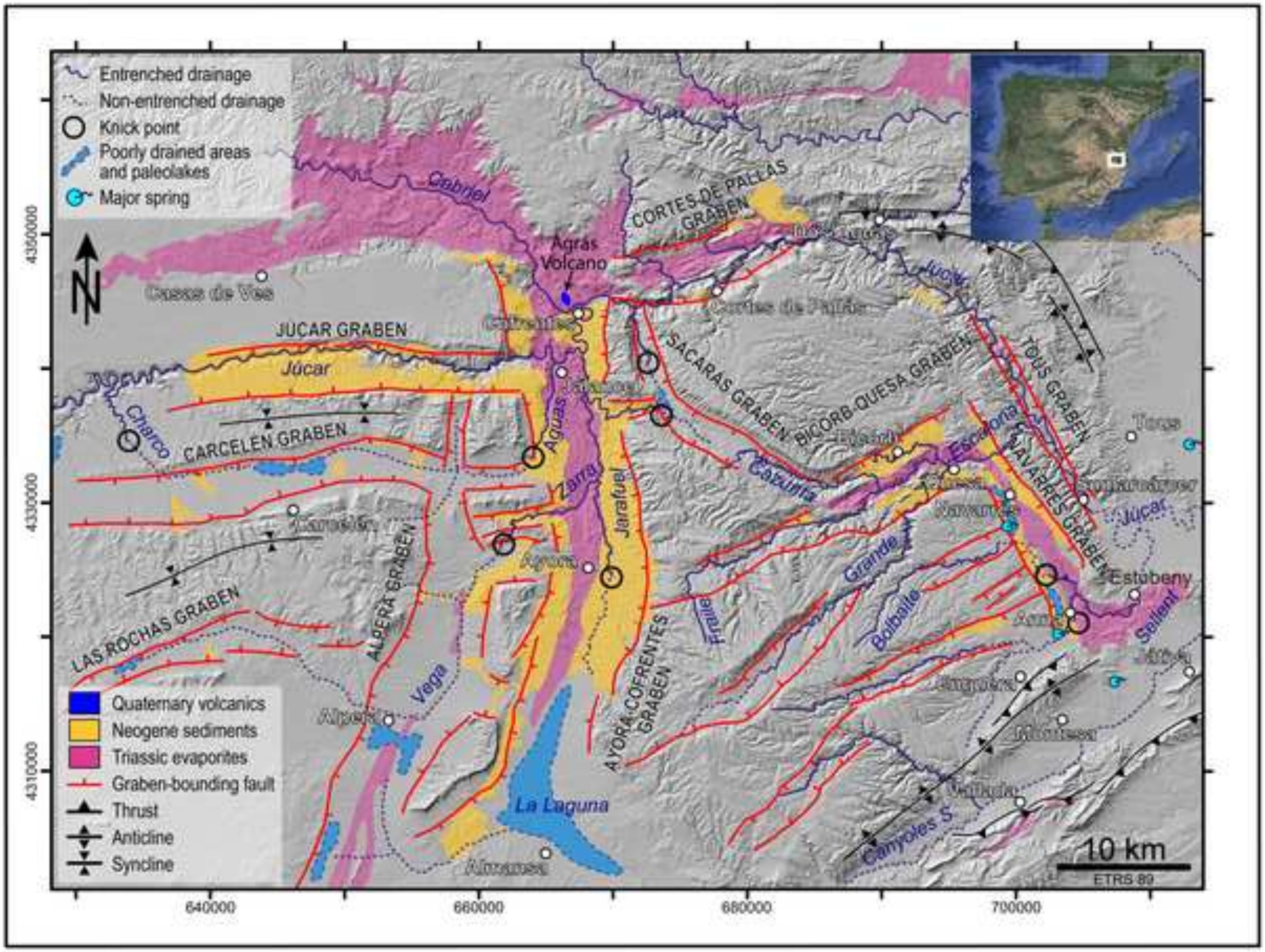

Figure (Color) 2

Click here to download high resolution image

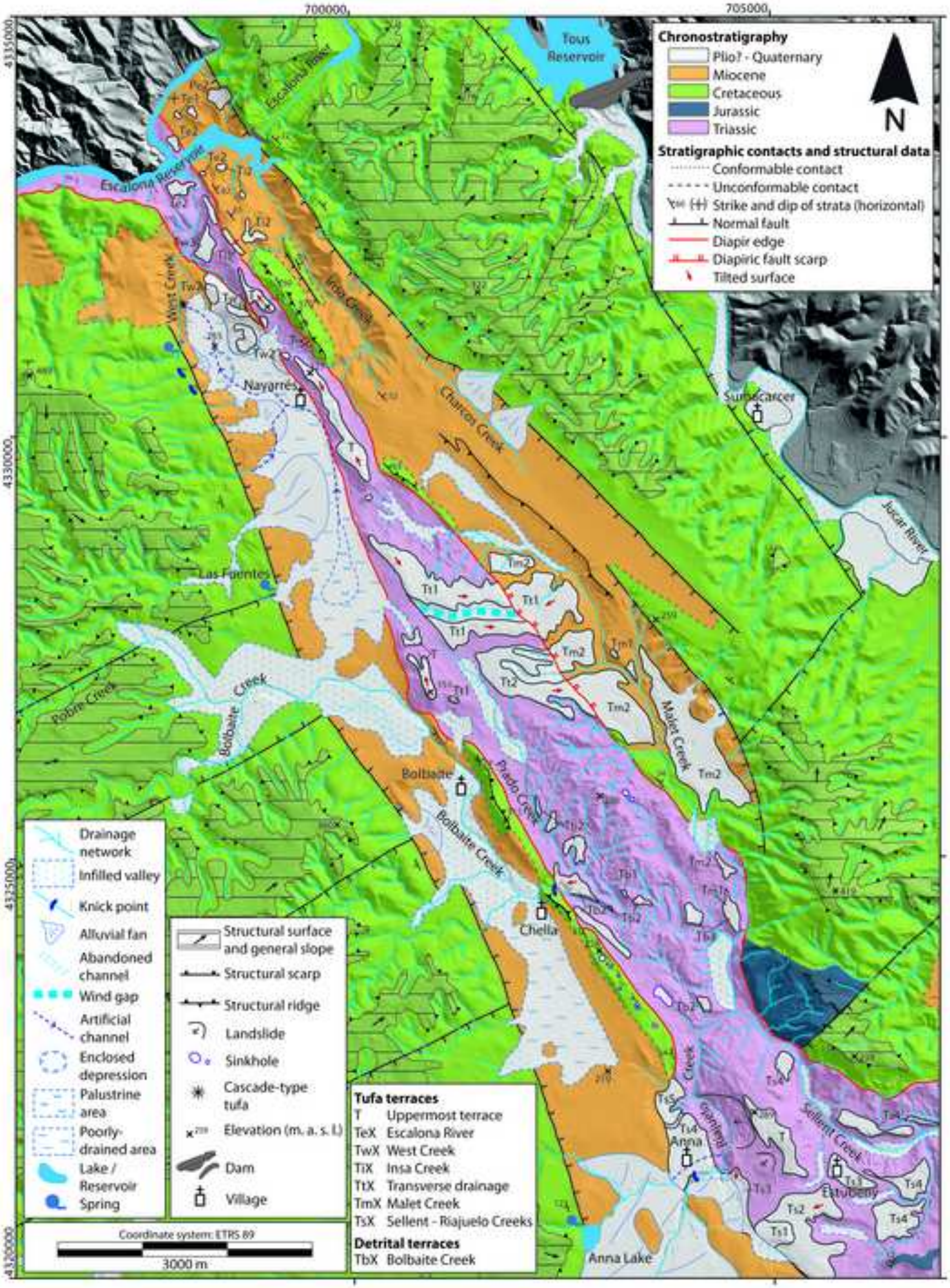

Figure (Color) 3

Click here to download high resolution image

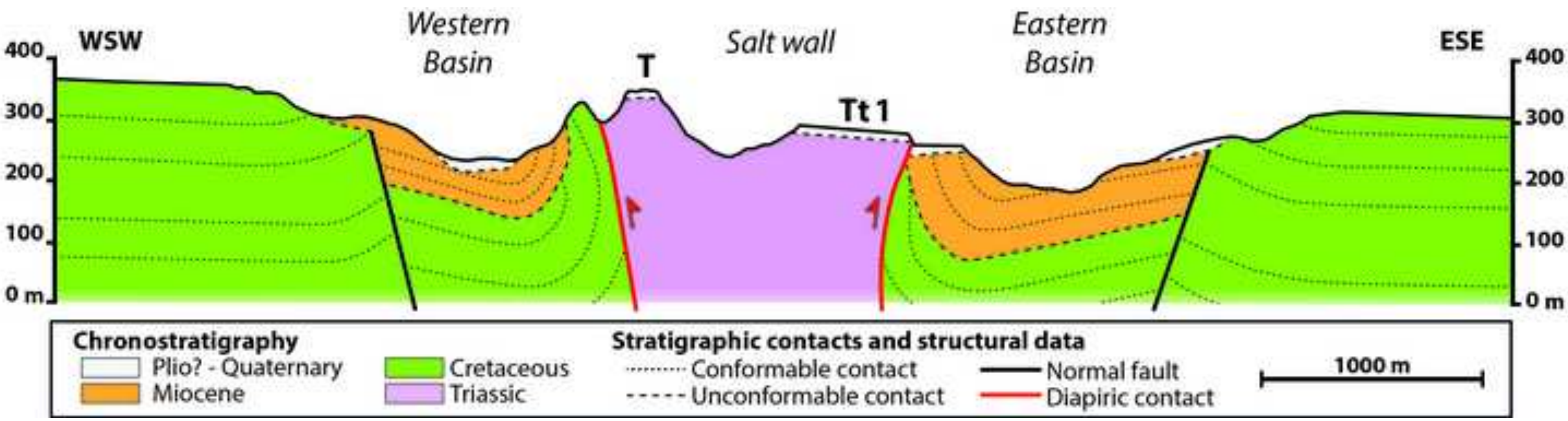

Figure (Color) 4
Click here to download high resolution image

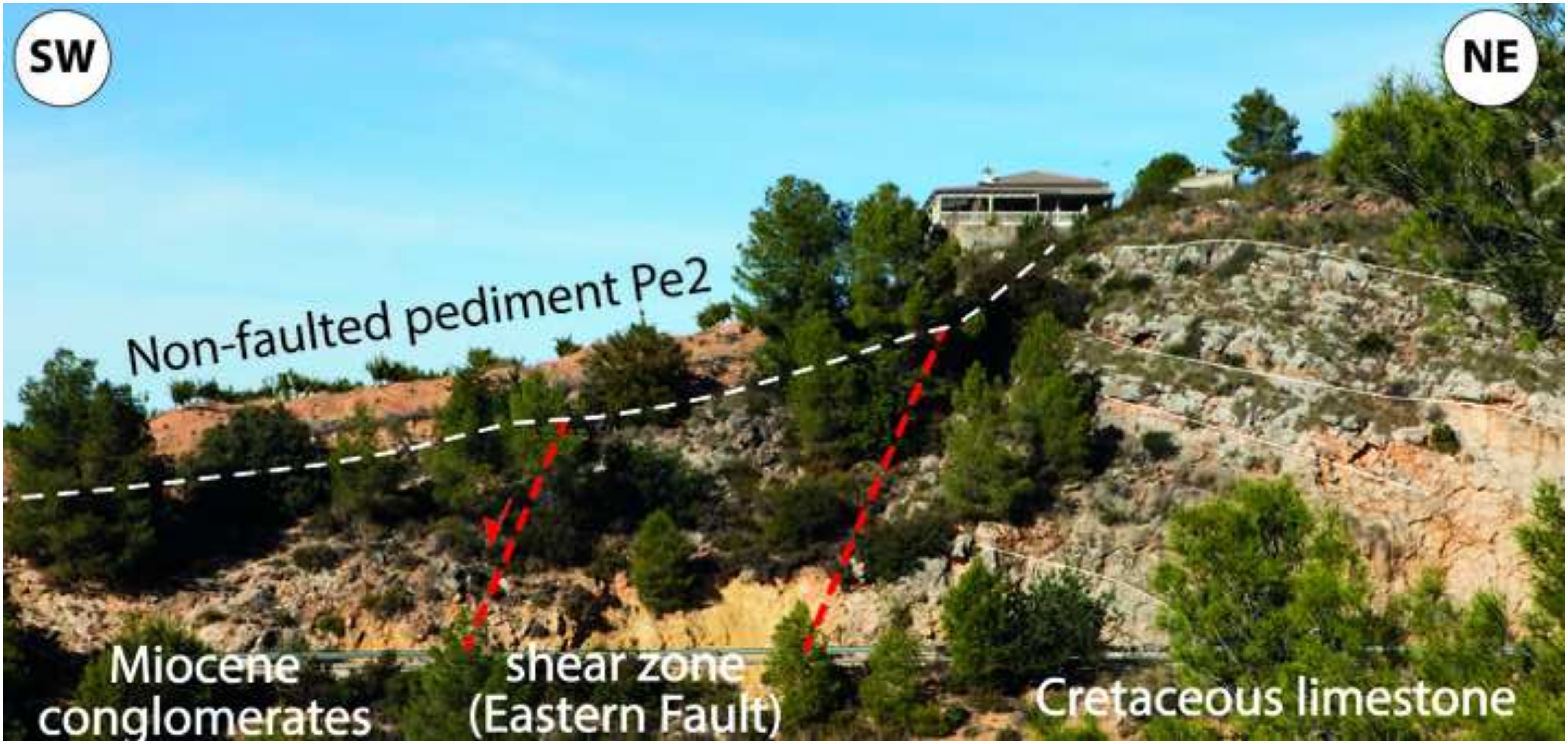

Figure (Color) 5
Click here to download high resolution image

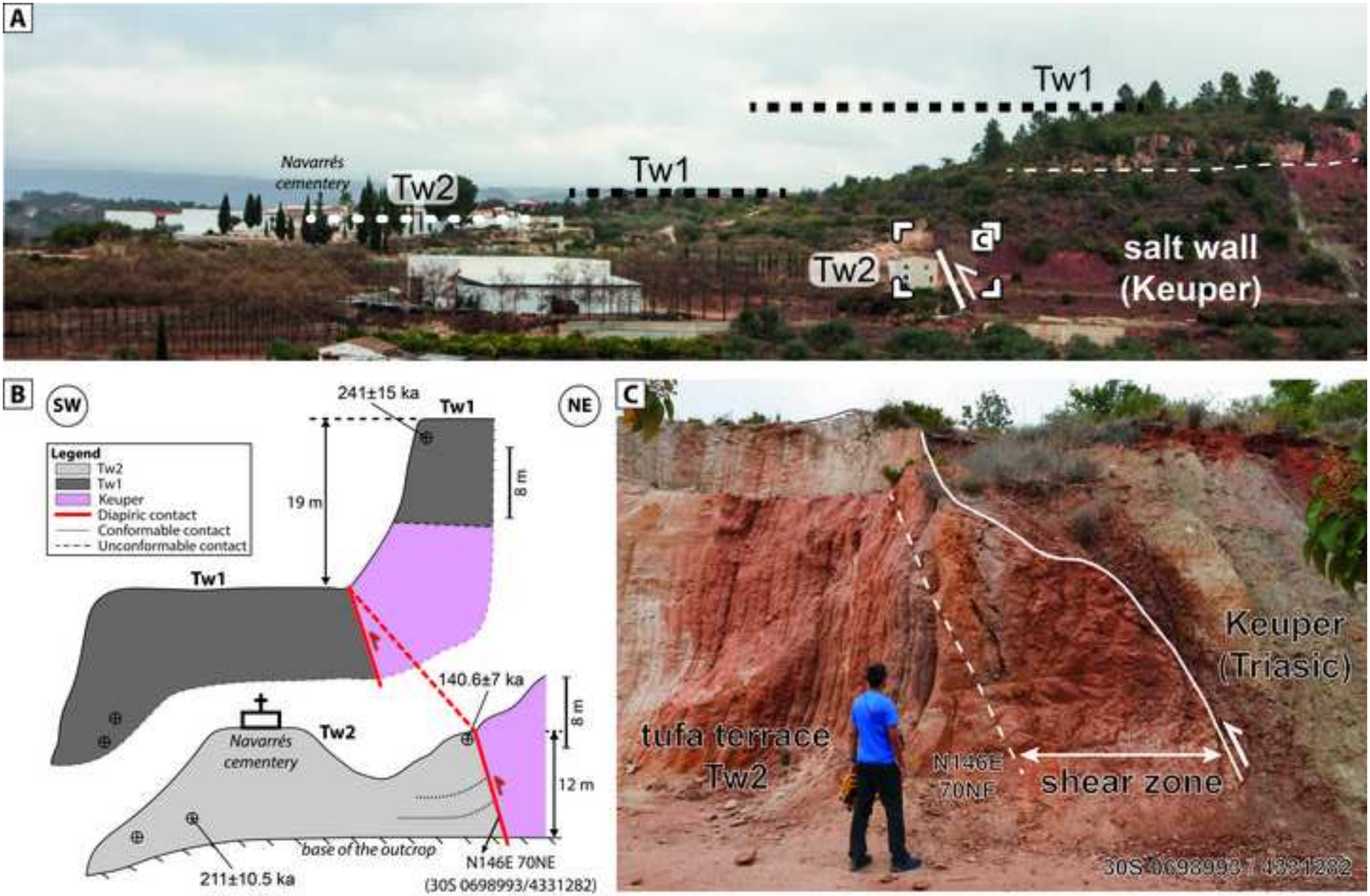

Figure (Color) 6
Click here to download high resolution image

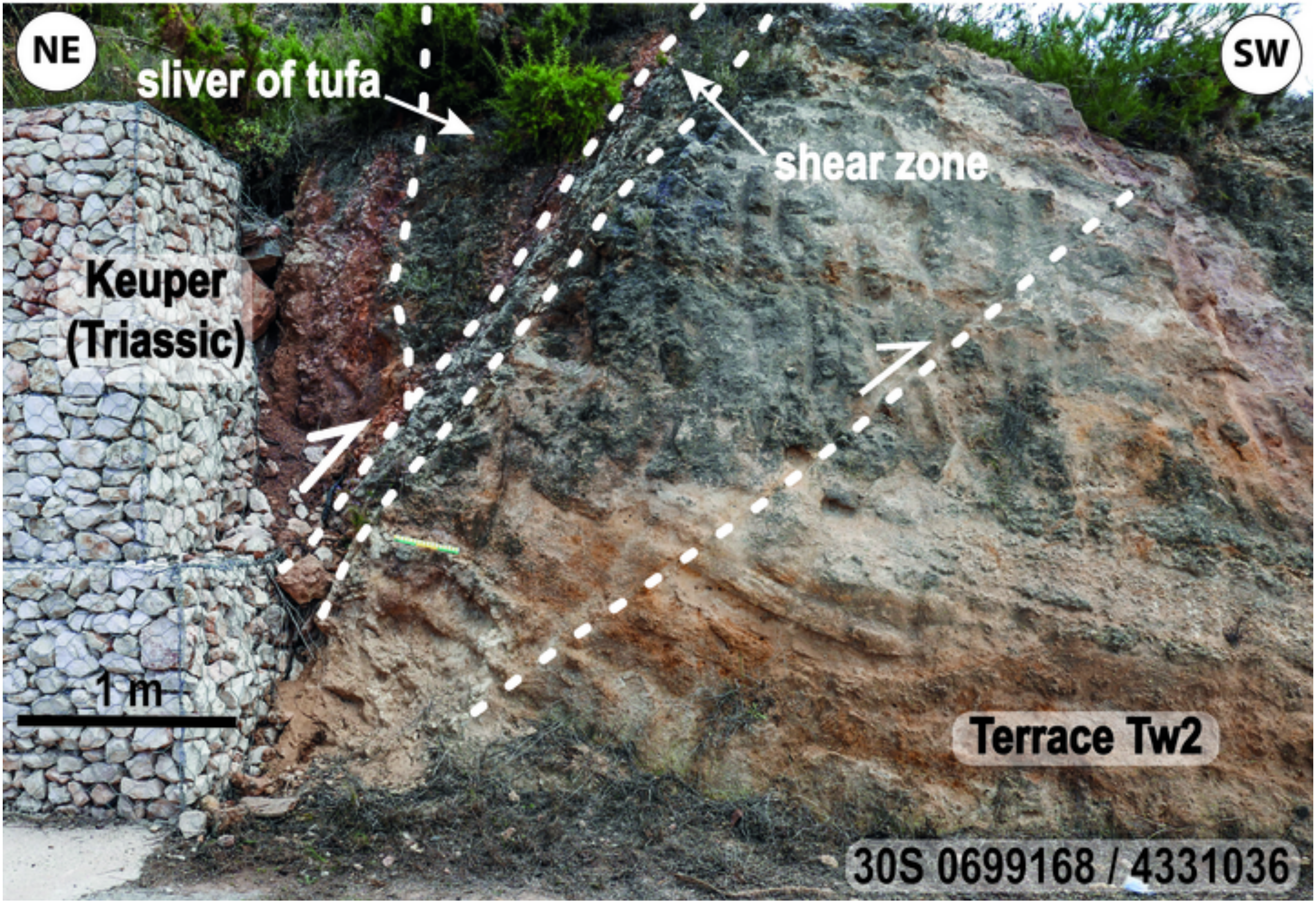

Figure (Color) 7
Click here to download high resolution image

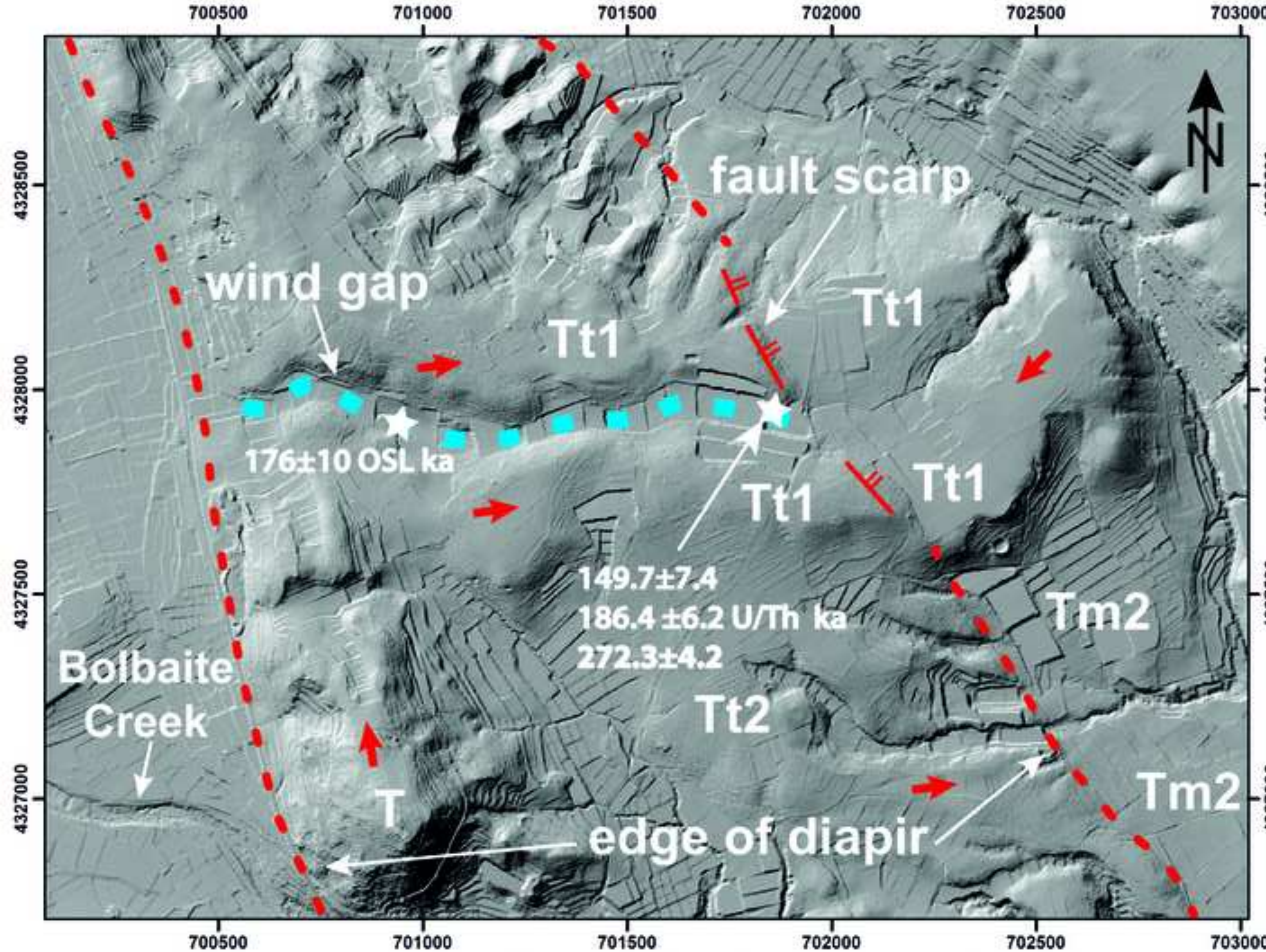

Figure (Color) 8
Click here to download high resolution image

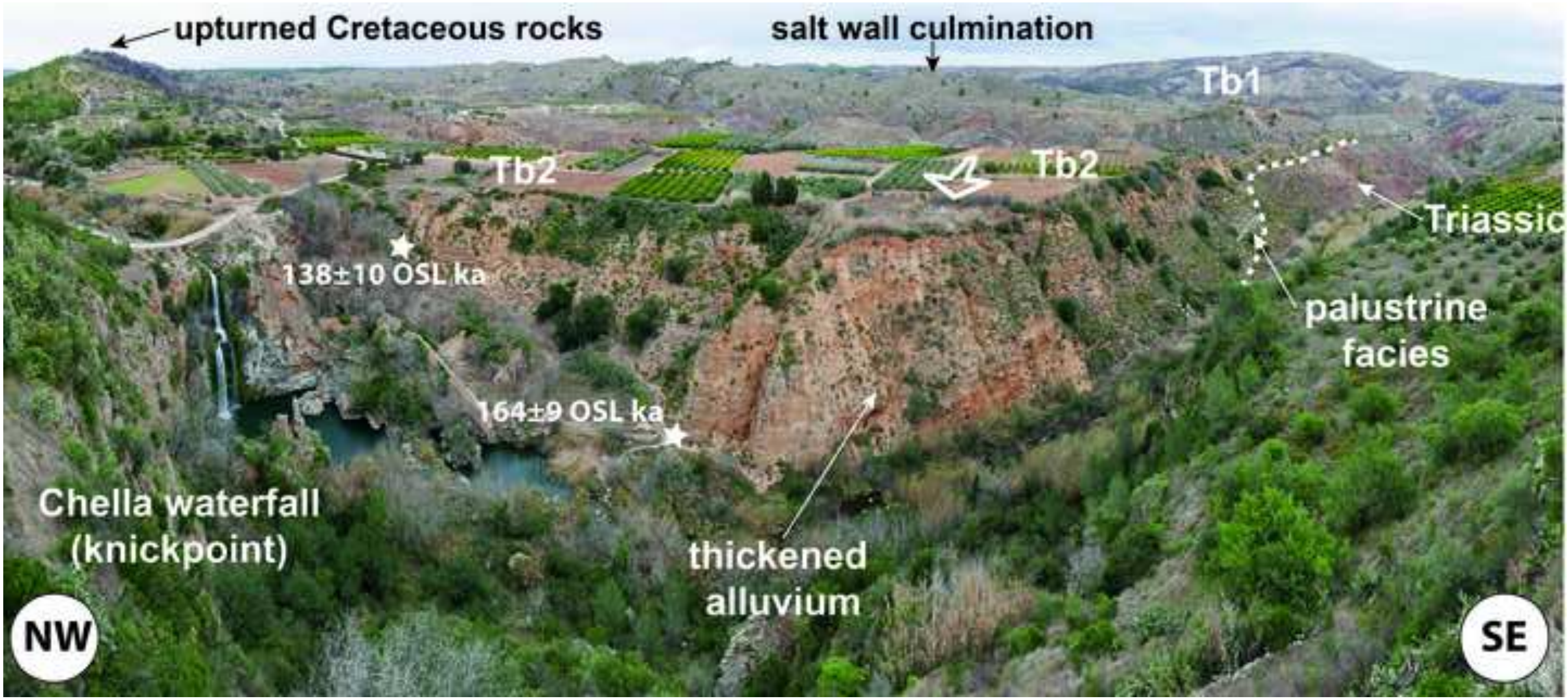

Figure (Color) 9
Click here to download high resolution image

Figure (Color) 10
Click here to download high resolution image

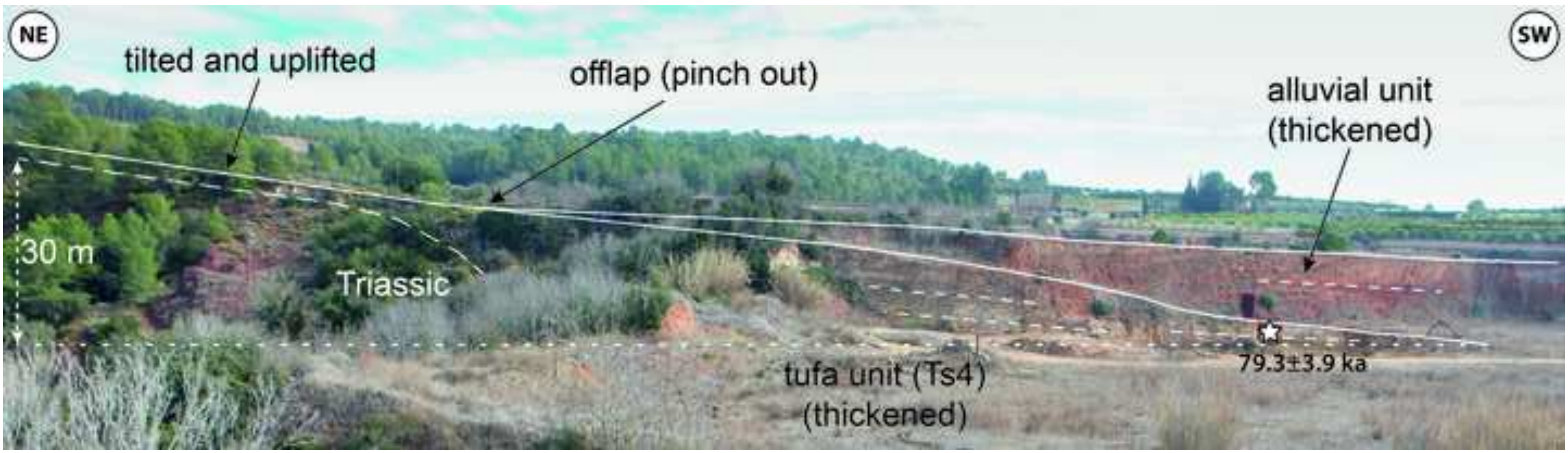

Figure (Color) 11
Click here to download high resolution image

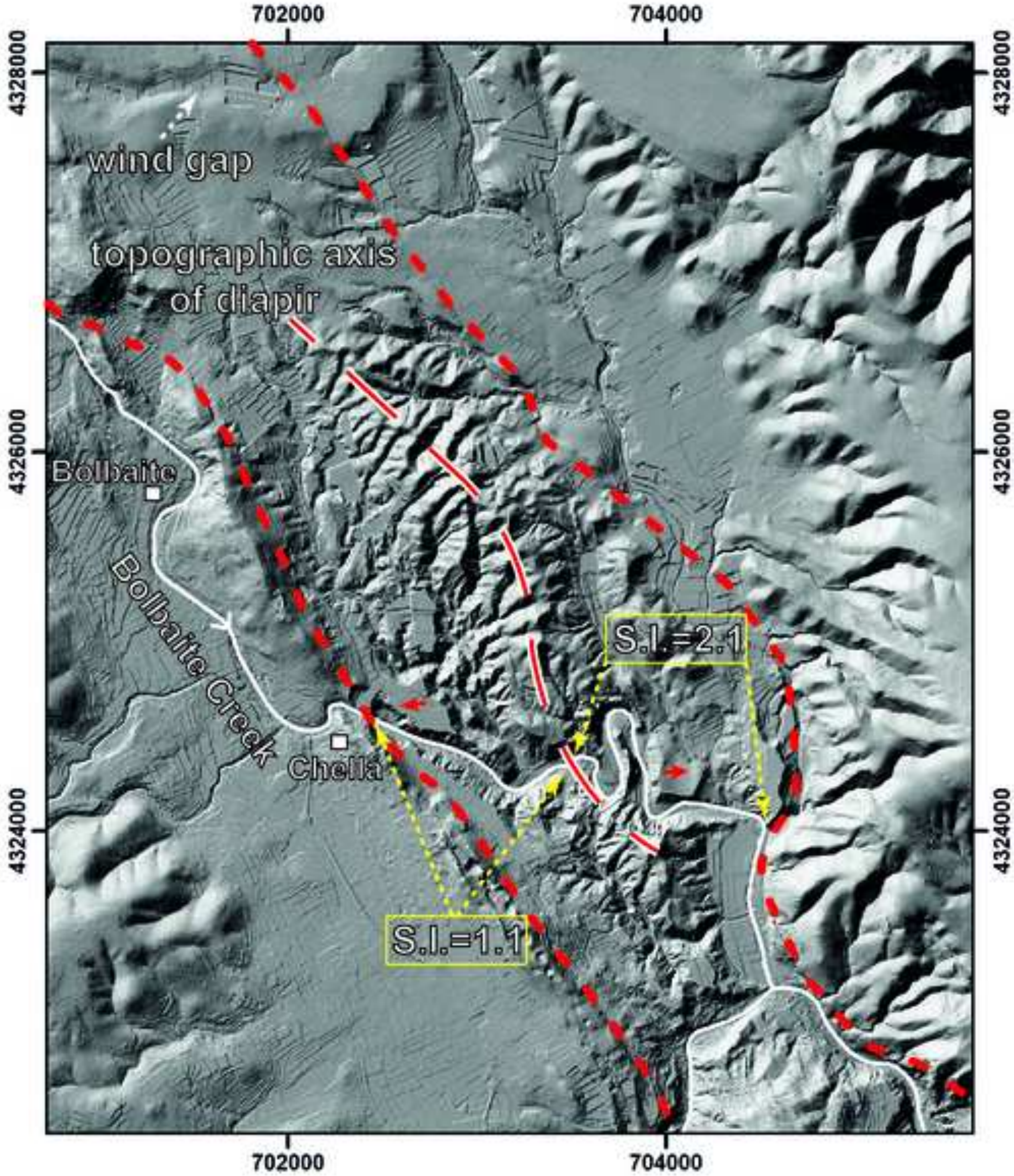

Figure (Color) 12
Click here to download high resolution image